

astro-ph/9812149
November 21, 2018

MHD waves as a source of matter density fluctuations within solar interior

N.S. Dzhaililov ¹ and V.B. Semikoz ²

*The Institute of the Terrestrial Magnetism, the Ionosphere and Radio Wave Propagation of the Russian Academy of Sciences
IZMIRAN, Troitsk, Moscow region, 142092, Russia*

Abstract

It is shown that in the presence of a background magnetic field within solar interior a cavity for low frequency MHD eigen modes (with periods 1-10 days) near equatorial plane can arise. The lower boundary of the cavity coincides with the center of the Sun while the upper one corresponds to the Alfvén resonant layer where high accumulation of wave energy takes place. The localization z_s and the width of the Alfvén resonance layer Δz_s are determined by: (i) the node number of eigen modes $n = 1, 2, \dots$, (ii) by the angle α of oblique propagation of waves with respect to the magnetic field \mathbf{B} , and (iii) by a low magnitude of the background magnetic field itself, $B_0 = 1 - 100$ G. The amplitude of eigen oscillations in a resonant layer determines the density fluctuation value $\delta\rho/\rho$ that is restricted through the imaginary part of eigen frequencies.

For large node numbers $n \gg 1$ there appear many narrow resonant layers where a neutrino propagates through a large density fluctuation $\delta\rho/\rho$ with the oscillation length that is much bigger than the width of a resonant layer, $l_{osc} = 4\pi E/\Delta m^2 \gg \Delta z_s(n)$. It is shown that neutrino crosses many such bumps on the exponential background profile that motivates to consider these MHD waves as a plausible matter noise for the MSW solution to the Solar Neutrino Problem (SNP).

PACS codes: 13.10.+q; 13.15.-f; 13.40.Fn; 14.60.Gh; 96.60.Kx.

Key words: neutrino, magnetic fields, magnetohydrodynamics, wave resonant absorption, cavity.

¹E-mail: namig@izmiran.rssi.ru

²E-mail: semikoz@orc.ru

1 Introduction

The existence of the solar neutrino problem is now established from five underground experiments [1, 2, 3, 4, 5] more or less independently of any details of the Standard Solar Model (SSM) [6].

At the same time it becomes clear [7] that any modifying SSM astrophysical solution contradicts the reconciled data of the Homestake [1] and the Kamiokande [2] experiments. Moreover, Helioseismology data are in a good agreement[8] with astrophysical parameter values given by SSM and relevant to all Particle Physics solutions: (i) neutrino vacuum oscillations [9], (ii) resonant neutrino oscillations in medium or the Mikheev-Smirnov-Wolfenstein (MSW) solution [10] and (iii) the Resonant Spin-Flavor Precession (RSFP) in medium[11].

The most popular Small Mixing Angle (SMA) MSW solution[10] depends on minimal number of unknown fundamental parameters (neutrino mass difference Δm^2 and mixing $\sin^2 2\theta \ll 1$) and relies on resonant neutrino conversions ($\nu_{eL} \rightarrow \nu_{\mu L}$) in matter with the smooth density profile $\rho_0 = \rho_{00} \exp(-r/H)$ where $H = 0.1R_{\odot}$ is the height scale in SSM [18]. Any change of this profile generally may be crucial for allowed fundamental parameter region (see below) while standard Helioseismology corrections to SSM give density fluctuations deep in the solar interior at the level $\delta\rho/\rho_0 \lesssim 1\%$ [12] that occurs too small to influence neutrino oscillations.

Another scenario (RSFP [11]) includes the additional parameter μB_0 where B_0 is an extrapolation of a regular large-scale magnetic field (as seen on the solar surface) down to the bottom of the convective zone and μ is an unknown transition Majorana (Dirac) neutrino magnetic moment. The existence of such large-scale magnetic fields B_0 under the bottom of the convective zone and even in the solar core is currently discussed (see, for instance, [13]), and it is not excluded that these fields can lead to the MHD wave generation in the solar interior relevant to the MSW-resonance region for neutrino oscillations since density perturbations $\delta\rho(\vec{r}, t)/\rho_0$ (as well as the magnetic field ones, $\vec{b}(\vec{r}, t)/B_0$, and the speed fluctuations $\vec{v}(\vec{r}, t)$) are evolved in the presence of a central field B_0 .

Therefore, the main goal of present work is the search of possible magnetic field enhancement of the density perturbations $\delta\rho/\rho_0$ resulting in an effective non-direct neutrino interaction with an external magnetic field B_0 *without any neutrino magnetic moment*. ³

³Another example of neutrino interaction with magnetic field and also without neutrino magnetic moment was found in [14] where the mean axial vector potential $V_A \sim G_F \langle \bar{\psi}_e \gamma_z \gamma_5 \psi \rangle \sim B_0$ for an electron gas polarized in a strong magnetic field $\mathbf{B} = (0, 0, B_0)$ [15] was calculated. This polarization leads to anisotropic neutrino emission through MSW oscillations studied in [16] in order to explain kick of a neutron star. For the solar case the axial vector potential is not efficient since the solar magnetic field is too small to polarize the Boltzman electron gas. Even at the bottom of the convective zone with the strongest magnetic field value $B_0 \sim 10^5$ G the paramagnetic contribution is $\mu_B B_0 \lesssim 10^{-3}$ eV only and the axial vector potential V_A is much less than the vector potential V ,

Here we consider only very modest values of large-scale background magnetic fields in central region of the Sun, $B_0 \sim 1 - 10 - 100 G$, that is not in contradiction with a primeval origin of such central field in the stars of main sequence like the Sun and with non-observation of traces of such small (dipole) fields in the solar photosphere. This is in contrast with the visible traces of more stronger toroidal (and poloidal) fields generated at the bottom of the convective zone.

In particular, the most interesting region $B_0 \lesssim 10 G$ where MHD density perturbations are similar to the intense matter noise (see below) obeys the constraint on the central field $B_0 \lesssim 30 G$ found recently [17] from the assumption of primeval origin of solar magnetic fields which are evolved via dynamo mechanism.

There were some previous attempts to modify the SSM density profile ρ_0 [18] entering the neutrino evolution equation in the MSW solution to SNP. The influence of periodic matter density perturbations above the average density ρ_0 , i.e.

$$\rho(r) = \rho_0[1 + h \sin(\gamma r)] , \quad (1)$$

on resonant neutrino conversion was investigated in Ref. [19]. In this case the parametric resonance effect appears when the fixed frequency (γ) of the perturbation is close to the neutrino oscillation frequency and a large amplitude value ($h \sim 0.1 - 0.2$) is assumed. There are also a number of works which address to similar effects by different approaches [20].

One of disadvantages of models like Eq. (1) is our unawareness of values of model parameters γ , h as well as of physical origin of these perturbations.

Another approach was developed in Ref.[21] where authors assumed the presence of a white noise of matter density ($\langle \xi \rangle = \langle \delta\rho/\rho_0 \rangle = 0$) added to ρ_0 instead of the second term in Eq. (1). The number of free parameters (the noise amplitude $\sqrt{\langle \xi^2 \rangle}$ and the correlation length L_0 for random δ -correlated domains) remains the same one ($=2$) while the presence of white noise in the Sun is doubtless since there are many mechanisms to enhance random density perturbations.

However, Bamert et al (c.f.,for instance, [22]) stated that in analysis of matter noise influence the MSW solution to SNP given in [21] (as well as in their own first work and in [23]) what has been missing so far is *a plausible source for such δ -correlated fluctuations in the vicinity of the MSW resonant point*.

Assuming that a certain superposition of g-modes can be a source of such fluctuations deep in the solar interior, they showed that even for large amplitudes of some g-modes (or large $\delta\rho/\rho \sim 4\%$) for a large size of density fluctuation cell, $L_0 \gtrsim 3000 km$, the direct numerical integration of evolution equation leads to standard MSW result.

Comparing this value with the neutrino oscillation length at the MSW resonance, $l_{osc}^{res} = l_v / \sin 2\theta = 250 km (E/MeV) / \Delta m_3^2 / \sin 2\theta$, they found that the main assumption of [21] about the δ -correlated form of matter density fluctuations, $L_0 \ll l_{osc}$,

$V_A \sim V \mu_B B_0 / T \ll V$ where the standard MSW vector potential is defined as $V = G_F \sqrt{2} \rho Y_e / m_p$ for $\nu_e \rightarrow \nu_\mu$ i.e. it is proportional to the mean matter density ρ . Here G_F is the Fermi constant, μ_B is the Bohr magneton, T is the temperature within the Sun, Y_e is the electron abundance.

is violated. Really, the opposite inequality holds, $L_0 \gg l_{osc}$, especially for typical g-mode wave lengths, $\lambda_g \sim L_0 \gtrsim 0.1R_\odot = 7 \times 10^4 \text{ km}$ if the scale of random domains is associated with a g-mode wave length.

Let us turn to the MHD waves trapping in cavities which are appearing in the central regions of the Sun as a result of simultaneous acting of magnetic fields and density inhomogeneities. There are two advantages of these oscillations: (i) accumulation of wave energy in a resonance Alfvén layer that leads to a large $\delta\rho/\rho_0$ (see below); (ii) short wave lengths $\lambda_{MHD} \ll l_{osc}$ that allows us to consider these waves as a source of δ -correlated matter noise.

First, notice that strictly speaking these MHD waves are called magneto-acoustic-gravity waves (MAG) [24] (see old bibliography therein). The spectrum of MAG waves is very wide and near the photosphere some of them can be trapped in the sub-photospheric waveguide with consequent transformation into the magnetosonic waves characterized by 3-5-min periods which indeed are observed in the active regions of the solar atmosphere.

We are interesting here in low-frequency branches of MAG waves which can lead to long periods (like days or weeks) for temporal variations of neutrino fluxes that, in general, can be observed in the SuperKamiokande (SK) experiment.

In the recent paper by Guzzo et al[25] it was found that in the presence of gravity force ideal magnetohydrodynamics (MHD) has a solution for magnetic field perturbation with the periods of a few days that correspond to slow and Alfvén waves, $\omega_S \sim \omega_A = kB_0/\sqrt{4\pi\rho(r)}$ where k is the wave number (free parameter obeying $k > 2\pi/R_\odot$, R_\odot is the solar radius), B_0 is a regular magnetic field in the Sun and $\rho(r)$ is the SSM matter density.

A search for such periodicity in SK could be, in principle, realized. However, the authors of[25] confined themselves with the statement that "...time fluctuations of the solar neutrino flux have to be observed if the resonant neutrino spin-flavor precession solution to the solar neutrino problem works".

In contrast to [25], we show that for the same MAG waves while one neglects neutrino magnetic moment or RSFP [11] is absent the MSW solution to SNP is nevertheless crucially modified and can lead to the corresponding temporal variations of neutrino flux.

In addition, the authors [25] did not calculate in a self-consistent way the location r_s and the width Δr_s of the singular (resonant) layer since they did not solve the eigen value problem on the base of solutions of the Heun equation (Eq. (15) below) or they did not find the corresponding MAG wave spectrum (including the imaginary part of frequency connected with Δr_s).

We show that low frequencies of eigen oscillations correspond to the resonant layer position deep in the solar interior (under the bottom of the convective zone) or a cavity for MAG waves being bounded by: (i) the center of the Sun and (ii) the Alfvén resonant layer is localized in the central region where matter density oscillations can influence the MSW resonance for neutrinos.

Note that large density fluctuations $\delta\rho/\rho_0$ in these narrow layers, $\Delta z_s \ll l_{osc}$, can influence the MSW conversions like a matter white noise[21] if these layers are tightly placed along neutrino trajectory.

This paper is organized as follows.

In section 2 we present the total set of MAG equations and derive the master Heun equation.

In section 3 we find asymptotic solutions of master equation near the center (subsection 3.1), at the surface of the Sun (subsection 3.2) and around the singular Alfvén layer (subsection 3.3).

In subsection 3.4.1 we discuss the cavity model in ideal MHD and collisionless damping of MAG waves in an Alfvén resonant layer. Then in subsections 3.4.2, 3.4.3 using reasonable boundary conditions from the common solution in whole region $0 \leq r \leq R_\odot$ we derive the dispersion relation for the discrete frequency spectrum $\omega_n(B_0, k_x, k_y)$. Here the order of modes $n = 1, 2, \dots$ enumerates the decomposition over the set of MAG eigen waves replacing Eq. (1) to

$$\rho(z, t) = \rho_0(z) [1 + \operatorname{Re} \sum_n \delta\rho_n(z, t) / \rho_0(z)] . \quad (2)$$

Then in section 4 we calculate the resonance layer location z_s and its width $\Delta z_s(n)$ making use of the wave energy flux bounded through imaginary part of eigen frequency.

In section 5 we present main results for matter density fluctuations that should be substituted into Eq. (2) and calculate the enhancement of a density perturbation $\delta\rho_n/\rho_0$ in a resonant Alfvén layer.

In final section 6 we discuss the validity of our results and state some problems for future exploration.

2 Master equation for MAG waves

For MAG waves we use the full set of MHD equations including the gravity force $\rho\vec{g}$ where $\vec{g} = \nabla\Phi$ and the gravity potential Φ is given by the Poisson equation $\Delta\phi = -4\pi G\rho$, $G \sim M_{Pl}^{-2}$ is the Newton constant.

The Euler equation (conservation of momentum) is of the form

$$\rho \frac{d\vec{v}}{dt} = -\nabla p + \rho\vec{g} + \frac{1}{4\pi} [\operatorname{rot} \vec{B} \times \vec{B}] , \quad (3)$$

where $d/dt = \partial/\partial t + \vec{v} \cdot \nabla$ is the substantial derivative and the last (Lorentz force) term may be transformed to the sum of the magnetic field pressure term $-\nabla B^2/8\pi$ and a perturbation magnetic field contribution $-(4\pi)^{-1}([\vec{b} \times [\nabla \times \vec{B}]] + [\vec{B} \times [\nabla \times \vec{b}]])$ when in linear MHD we decompose the total field $\vec{B} = \vec{B}_0 + \vec{b}(t, \vec{r})$ (see below subsection 2.1).

The mass conservation leads to the continuity equation

$$\frac{d\rho}{dt} + \rho u = 0 . \quad (4)$$

Here for compressible gas the function $u = \text{div } \vec{v} \neq 0$ is the main object for search of solutions with MAG waves. We decompose density in linear MHD as $\rho = \rho_0 + \delta\rho(t, \vec{r})$ with the background density ρ_0 given by SSM [18].

The energy conservation obeys

$$\frac{dp}{dt} - \gamma \frac{p}{\rho} \frac{d\rho}{dt} = -(\gamma - 1)Q , \quad (5)$$

where the factor $\gamma = c_p/c_V$ is given by the heat capacities, Q is the rate of all energy density sources and losses.

Finally system is completed by the Faradey equation for the magnetic field,

$$\frac{\partial \vec{B}}{\partial t} = \text{rot} [\vec{v} \times \vec{B}] + \frac{c^2}{4\pi\sigma} \Delta \vec{B} ,$$

that transits in ideal MHD (the conductivity $\sigma \rightarrow \infty$) to the equation for *frozen-in* magnetic field,

$$\frac{\partial \vec{b}}{\partial t} = \nabla \times [\vec{v} \times \vec{B}_0] . \quad (6)$$

In the last equation we assumed that the background field B_0 does not depend on time.

Obviously, these equations transit to the Standard Helioseismology Model (SHM) equations in the limit $B \rightarrow 0$.

The system of linearized Eqs. (3-6) for non-adiabatic perturbations in a compressible ideal conducting medium with arbitrary direction of the magnetic field \mathbf{B} and in the Cowling approximation (neglecting the perturbation of the gravitational potential, $\delta\phi = 0$) is reduced to

$$\begin{aligned} \frac{\partial \delta\rho}{\partial t} + (\vec{v} \nabla) \rho_0 + \rho_0 u &= 0 , \\ \rho_0 \frac{\partial \vec{v}}{\partial t} + \nabla \delta p - \vec{g} \delta\rho + \frac{1}{4\pi} [\nabla (\vec{B}_0 \vec{b}) - (\vec{B}_0 \nabla) \vec{b}] &= 0 , \\ \rho_0 c_V \left[\frac{\partial \delta T}{\partial t} + (\vec{v} \nabla) T_0 \right] + p_0 u &= \delta Q , \\ \frac{\partial \vec{b}}{\partial t} - (\vec{B}_0 \nabla) \vec{v} + \vec{B}_0 u &= 0 , \\ \frac{\delta p}{p_0} &= \frac{\delta\rho}{\rho_0} + \frac{\delta T}{T_0} . \end{aligned} \quad (7)$$

Here \vec{v} , δT , $\delta \rho$, δp and \vec{b} are small Euler perturbations of the velocity, the temperature, the density, the pressure and the magnetic field strength correspondingly. One supposes that at initial state the gas is immovable ($\vec{v}_0 = 0$) and for the constant magnetic field B_0 the ideal gas ($p_0 = R\rho_0 T_0$) obeys the hydrostatic equilibrium, $\nabla p_0 = \rho_0 g$. Notice that fifth equation in (7) follows from equation of state of ideal gas.

In what follows we consider the wave dynamics in central regions of the Sun where the adiabatic condition, $\delta Q = 0$, is fulfilled with good accuracy for the high frequency oscillations in SHM and MHD. To simplify the further analysis we adopt this condition for whole spectrum of oscillations in MHD.

Since we assume the background magnetic field \vec{B}_0 has the dipole structure one expects that it occurs both constant and uniform near the dipole axis or we can put $B_0 = \text{const}$ within central region of the Sun where a cavity for eigen MAG oscillations is localized. In addition to, since neutrinos propagate to the Earth along the ecliptic one can suppose that the dipole magnetic field is perpendicular to the direction of neutrino momentum.

Thus, we choose the Cartesian coordinate system with z-axis directed upon opposite direction to the neutrino momentum or along \vec{g} . This means: (i) $z = 0$ at the surface of the Sun and (ii) $z = R_\odot$ at its center. In this system the magnetic field and acceleration vectors are $\vec{B}_0 = (B_0, 0, 0)$, $\vec{g} = (0, 0, g(z))$.

In order to obtain an analytical solution of the system Eq. (7) we adopt additional assumptions based on an effective short wave length along z-axis, $\lambda_z \ll H_\rho = |(1/\rho_0)d\rho_0/dz|^{-1}$ where $H_\rho \equiv H = 0.1R_\odot = \text{const}$ is the density height scale[18]. Really in most interesting cases of cavities in deep solar interior the MHD wave spectrum ω_n depends on large order (node) numbers $n \gg 10$ with the effective wave length $\lambda_z \sim L/n$ where $L \simeq z_s \leq R_\odot$ is the cavity width, z_s is the Alfvén resonant layer position (see below section 4).

On the other hand, using the real model of the Sun [26] one can easily show that both the temperature $T_0(z)$ and the acceleration $g(z)$ have large height scales, $H_T = |(1/T_0)dT_0(z)/dz|^{-1}$ and $H_g = |(1/g)dg(z)/dz|^{-1}$ correspondingly, obeying the inequalities $H_g, H_T > H_\rho$. As result we may consider the gravity force acceleration g and the temperature T_0 as some constants on scales of MHD wave lengths, $g \approx \text{const}$, $T_0 \approx \text{const}$. This approximation remains valid even on whole cavity width L for "narrow" cavities $3H \lesssim L \lesssim H_T$, H_g including the MSW resonant point $r_{MSW} \sim 0.3R_\odot$ in the solar interior while it fails near the center of the Sun, $z \ll H_\rho$, where $g \sim z$.

The isothermal approximation with $g \approx \text{const}$ means that the density and the pressure are given by the exponential (Boltzman) law: $\rho_0 \sim e^{z/H}$, $p_0 \sim e^{z/H}$ obeying the ideal gas equation state $p_0/\rho_0 = RT_0/\mu$ with the gas constant $R = \kappa/m_u$ and the molecular weight μ measured in mass units $m_u \simeq m_p$. Here κ is the Boltzman constant; $H = c^2/g = \text{const}$ is the height scale[18]; $c = \sqrt{RT_0/\gamma\mu} = \text{const}$ is the isothermal sound velocity and the adiabatic sound velocity is given by $c_s^2 = \gamma c^2 = \text{const}$.

Thus we are looking for solutions in the form $\vec{v} = \vec{v}(z) \exp(-i(\omega t - k_x x - k_y y))$ (and analogously for $\delta\rho$ and \vec{b}). We keep here notations of the paper [27]. In these notations we obtain from the system (7) all perturbation functions. In particular, velocity perturbations are of the form

$$v_x = -\frac{ik_x(c_s^2 u + gv_z)}{\omega^2}, \quad (8)$$

$$v_y = \frac{-ik_y}{\omega^2} \left[gv_z + \left(c_s^2 + \frac{v_A^2 \omega^2}{\omega^2 - k_x^2 v_A^2} \right) u \right], \quad (9)$$

$$\begin{aligned} v_z = & \left(\frac{\omega^2 g}{k_\perp^2 g^2 - \omega^4} \right) \times \\ & \times \left\{ \left[1 - \frac{k_\perp^2 c_s^2}{\omega^2} + \frac{\omega^2(\gamma - 1) - k_y^2 v_A^2}{\omega^2 - k_x^2 v_A^2} \right] u + \right. \\ & \left. + \left(c_s^2 + \frac{\omega^2 v_A^2}{\omega^2 - k_x^2 v_A^2} \right) \frac{1}{g} \frac{du}{dz} \right\}. \end{aligned} \quad (10)$$

From the continuity equation Eq. (4) or from the first equation in (7) we have obtained the density perturbation,

$$\frac{\delta\rho}{\rho_0} = \frac{1}{i\omega} \left[u + \frac{v_z}{H} \right], \quad (11)$$

and from Maxwell equations for ideal plasma Eq. (6) or from the fourth equation in (7) we find magnetic field perturbations,

$$b_x = -\frac{k_x v_x}{\omega} B_0 + \frac{u}{i\omega} B_0, \quad (12)$$

$$b_y = -\frac{k_x v_y}{\omega} B_0, \quad (13)$$

$$b_z = -\frac{k_x v_z}{\omega} B_0. \quad (14)$$

One can easily see from Eqs. (8)-(14) that all perturbation functions are expressed via one unknown function $u(z) = dv_z/dz + ik_x v_x + ik_y v_y$.

The master equation for $u(z)$ follows from last definition and coincides ⁴ with Eq. (3) in [27]

$$\begin{aligned} & (\xi - 1)(\xi - a)\xi \frac{d}{d\xi} \xi \frac{du}{d\xi} + \xi^2(\xi - 2 + a) \frac{du}{d\xi} + \\ & + \{\xi \left[(\xi - 1)b + K_\perp^2 \left(a + \frac{1}{\gamma K_x^2} \right) - 1 \right] - K_\perp^2 a\} u = 0, \end{aligned} \quad (15)$$

⁴ More than hundred years this equation for an arbitrary argument ξ is known in mathematics as the Heun equation [28].

where $\xi = \omega^2/k_x^2 v_A^2$ is the independent variable; $v_A(z) = B_0/\sqrt{4\pi\rho_0(z)}$ is the Alfvén velocity; $K_\perp = \sqrt{K_x^2 + K_y^2}$ and ω are the transversal wave number and the oscillation frequency correspondingly.

The dimensionless parameters in Eq. (15) are given by

$$\begin{aligned} a &= 1 - \frac{\Omega^2}{\gamma K_x^2}, \quad b = \frac{\Omega^2}{\gamma} + K_\perp^2 \left(\frac{\gamma - 1}{\gamma \Omega^2} - 1 \right), \\ \Omega &= \frac{\omega H}{c}, \quad K_x = k_x H, \quad K_y = k_y H, \\ \xi &= \frac{\Omega^2}{\gamma K_x^2} \beta(z); \quad \beta(z) = \frac{c_s^2}{v_A^2} = \beta_0 e^{z/H}. \end{aligned} \quad (16)$$

Eq. (15) is the ordinary differential equation of the second order with four singular points: $\xi = 0, 1, a, \infty$. The solutions of this equations are given by the Heun functions[28]. These solutions were explored in the paper[27], however, they are too complicated for application to solar neutrino physics.

Therefore, we have simplified Eq. (15) in order to find solutions through elementary functions and to study main physical properties of the MAG wave cavity within solar interior.

In general, when both $K_x \neq 0$ and $K_y \neq 0$, the master equation Eq. (15) has two singular levels: the resonance level $\xi = a$ arises for the condition $\omega^2 = c_s^2 v_A^2 k_x^2 / (c_s^2 + v_A^2)$ (*casp resonance*) and the condition $\xi = 1$ is fulfilled for $\omega^2 = k_x^2 v_A^2$ (*Alfvén resonance*).

As shown in [27] for the solar conditions the casp resonance level lies in medium above the Alfvén level, however, the distance between these levels, $\Delta z_{Acasp} = H \ln[1 - \Omega^2/\gamma K_x^2]^{-1}$ is negligible for low frequencies $\Omega \ll \gamma K_x^2$ because we are interesting in 1-10 days variations of density fluctuations with the probable influence neutrino flux.

When waves reach resonance level which has a finite width in z-direction and is infinite in both perpendicular directions they can be efficiently absorbed within resonant layer. This leads to concentration of wave energy along magnetic field. The energy absorption coefficient is of the form ⁵ [24]

$$D = 1 - \exp(-2\pi\sqrt{4b - 1}), \quad (17)$$

or absorption becomes more efficient for low frequencies, $\Omega \rightarrow 0, b \rightarrow \infty, D \rightarrow 1$.

The coincidence of casp resonant layers with the Alvenic ones for low frequencies ($\Omega \ll \gamma K_x^2$) means that the resonant layer $\xi = 1$ may appear only within the Sun where the condition $v_A \ll c_s$ is fulfilled that corresponds to the inequality for gas and magnetic field pressures, $p_{gas} = p_0 \gg p_{mag} = B_0^2/8\pi$.

In such conditions we can simplify our master equation Eq. (15) that can be written in the final form

$$(\xi - 1)^2 \xi \frac{d}{d\xi} \xi \frac{du}{d\xi} + \xi^2 (\xi - 1) \frac{du}{d\xi} +$$

⁵In this formula one neglects the temporal decay of a wave amplitude since free oscillations without lower reflector and thereby with zero imaginary part of the frequency $Im \Omega = 0$ are assumed.

$$+\{\xi\left[(\xi-1)b+K_{\perp}^2\left(1+\frac{1}{\gamma K_x^2}\right)-1\right]-K_{\perp}^2\}u=0. \quad (18)$$

Here one supposes also $\gamma \approx const$.

3 Asymptotic solutions

The main idea how to find simple asymptotic solutions of Eq. (18) comes from its physical simplifications in three important regions: near the photosphere $z = 0$, $|\xi| \ll 1$, around the singular (Alfvén) layer $|\xi - 1| < 1$ and near the center of the Sun, $z = R_{\odot}$ where $|\xi| \gg 1$ for the same fixed frequency ω . In these regions solutions are expressed through elementary functions. Using conditions of linear dependence of these regional solutions we build a more general solution that is valid in whole region $-\infty < z < \infty$.

Then using boundary conditions at the center of the Sun and at the solar surface we have found eigen frequencies (subsection 3.4).

3.1 Solution near center of the Sun

In central region of the Sun for $|\xi| > 1$ including the center, $z_s \leq z \leq R_{\odot}$, where the resonant Alfvén layer position z_s is given by the value $(\omega/k_x v_A(z_s))^2 = \xi = 1$ we can reduce Eq. (18) to the more simpler form

$$\xi^2 \frac{d^2 u}{d\xi^2} + 2\xi \frac{du}{d\xi} + bu = 0. \quad (19)$$

General solution of this equation is of the form

$$u = u_1 = \frac{1}{\sqrt{\xi}} (A_1 \xi^{i\nu} + A_2 \xi^{-i\nu}), \quad (20)$$

where $\nu = \sqrt{b - 1/4} \approx (K_{\perp}/\Omega)\sqrt{(\gamma - 1)/\gamma}$, $A_{1,2}$ are arbitrary constants which are determined from boundary conditions. For low frequencies $|\nu| \gg 1$ the derivative is substituted by

$$\frac{du_1}{d\xi} \approx \frac{i\nu}{\xi \sqrt{\xi}} (A_1 \xi^{i\nu} - A_2 \xi^{-i\nu}). \quad (21)$$

Since the variable ξ is proportional to the SSM density profile $\xi \sim e^{z/H}$ [18] the solution Eq. (20) describes the incident wave and the reflected one with the wave number $k_z = \nu/H$.

One can easily see that the asymptotic Eq. (19) is similar with the SHM equation for g-modes where the wave number $b/H^2 \approx k_x^2 g(\gamma - 1)/\gamma H \omega^2$ in Eq. (16) includes the buoyancy frequency term $N^2/\omega^2 \sim g(\gamma - 1)/H \omega^2$ coming in SHM equations. This corresponds to the limit $B_0 \rightarrow 0$ when the variable ξ increases ($\xi \rightarrow \infty$).

3.2 Solution in vicinity of a resonant Alfvén layer

For $\xi \rightarrow 1$ Eq. (18) transits to

$$(\xi - 1)^2 \frac{d^2 u}{d\xi^2} + (\xi - 1) \frac{du}{d\xi} + \\ + \left[(\xi - 1) \frac{(\gamma - 1)}{\gamma} \frac{K_\perp^2}{\Omega^2} + \frac{K_\perp^2}{\gamma K_x^2} - 1 \right] u = 0. \quad (22)$$

Two linear independent solutions of this equation are expressed through the Bessel functions of the 1-st kind:

$$u = u_2 = C_1 J_\mu(\Psi) + C_2 J_{-\mu}(\Psi), \quad (23)$$

where we denoted the argument and the index of Bessel functions as $\Psi = 2\nu\sqrt{\xi-1}$, $\mu = 2[1 - K_\perp^2/\gamma K_x^2]^{1/2}$ correspondingly and $C_{1,2}$ are arbitrary constants.

For the case of MAG wave propagation along magnetic field ($k_y = 0$) the index μ is real, $\mu^2 = 4(\gamma - 1)/\gamma$, while for the particular case of oblique wave propagation $k_y/k_x = \sqrt{15\gamma/16 - 1} = 3/4$ (ideal H-atomic gas, $\gamma = 5/3$) the real index $\mu = 1/2$ corresponds to the trigonometrical functions instead of the Bessel ones,

$$u_2 = \sqrt{\frac{2}{\pi\Psi}} [C_1 \sin \Psi + C_2 \cos \Psi]. \quad (24)$$

As it follows from the decomposition of Bessel functions near the resonance level $\xi \approx 1$, or explicitly for the particular case (24) the second independent solution diverges in the limit $\xi \rightarrow 1$. However, since this singular behaviour is an intrinsic property of the solution Eq. (23) caused by physical reasons we may not exclude this singularity by the forced condition $C_2 = 0$. It is important for our problem to have convergence (regular solution) in all points along integration path $|z| \rightarrow \infty$. An analytic continuation (transition to the complex argument $\xi = \xi_1 + i\xi_2$) originated by a physical mechanism discussed below means that $\xi = 1$ is the removable singularity.

Notice that the solution Eq.(23) is oscillating along the direction to the center, $\xi \gtrsim 1$, and has exponential behaviour in opposite direction (to the surface of the Sun), $\xi \lesssim 1$. First derivative of the solution Eq. (23) is of the form

$$\frac{du_2}{d\xi} = \frac{2\nu^2}{\Psi} [C_1 J'_\mu(\Psi) + C_2 J'_{-\mu}(\Psi)], \quad (25)$$

where $J'_\mu(\Psi) = (\mu/\Psi) J_\mu(\Psi) - J_{\mu+1}(\Psi)$.

3.3 Solution near surface of the Sun

The argument $\xi = \omega^2/(k_x^2 v_A^2)$ in Eq. (16) is given by the parameter $\beta = \beta_0 e^{z/H}$ where near the solar surface $z = 0$ the factor β_0 is changing in a wide region[29]

$$\beta_0 = \begin{cases} 40, & \text{for } B = 1000 \text{ G,} \\ 400, & \text{for } B = 100 \text{ G,} \\ 40000, & \text{for } B = 10 \text{ G.} \end{cases} \quad (26)$$

However, for any β_0 and $K_x \geq 1$ the argument ξ occurs small near photosphere, $|\xi| \ll 1$, since we have considered low frequencies through whole solar interior, $\omega \lesssim 10^{-5} \text{ s}^{-1}$. As result the master equation Eq. (18) transits near photosphere to

$$\xi^2 \frac{d^2 u}{d\xi^2} + \xi \frac{du}{d\xi} - \left(\xi \frac{\gamma - 1}{\gamma} \frac{K_\perp^2}{\Omega^2} + K_\perp^2 \right) u = 0, \quad (27)$$

which has the solution

$$u = u_3 = D_1 J_{2K_\perp}(y) + D_2 J_{-2K_\perp}(y). \quad (28)$$

Here the Bessel functions depend on the argument $y = 2\nu\sqrt{-\xi}$, $D_{1,2}$ are new integration constants. The demand of regularity of the solution Eq. (28) on the photosphere, $\xi \rightarrow 0$, results in $D_2 = 0$. The solution Eq. (28) describes evanescent oscillations with an exponential decreasing amplitude at the surface of the Sun.

The derivative of the solution Eq. (28) is given by

$$\frac{du_3}{d\xi} = -D_1 \frac{2\nu^2}{y} \left[\frac{2K_\perp}{y} J_{2K_\perp}(y) - J_{1+2K_\perp}(y) \right]. \quad (29)$$

3.4 Spectrum of MAG waves

3.4.1 Cavity model in ideal MHD

We have shown that the Alfvén resonant level $\xi = 1$ divides whole wave propagation space into two parts in which MHD waves have distinct properties. In the region $1 < \xi < +\infty$ the solutions $u_1(\xi)$ and $u_2(\xi)$ describe waves that propagate in both directions along z -axis while in the region $0 \leq \xi < 1$ the solutions $u_2(\xi)$ and $u_3(\xi)$ describe evanescent oscillations that decrease in an exponential way to the surface of the Sun, $z = 0$. The level $\xi = 1$ itself is the singular level where $u_2(\xi) \rightarrow \infty$.

Therefore, waves which are propagating from the center of the Sun reach the resonance level $\xi = 1$ where their partition implies reflection back and partial capture at the resonance layer. In general, high wave amplitudes at the resonance imply a

start-up of different dissipation mechanisms (linear or non-linear) within that layer. The condition $v_z = 0$ for the hard center of the Sun is a natural demand due to high pressure there and leads to full wave reflection from the center resulting in a cavity appearance with the lower boundary at the center $z = R_\odot$ and the upper boundary $z = z_s$ at the Alfvén resonance layer.

The cavity is defined within the region $1 \leq \xi \leq \xi_\infty$ and its width $L = H \ln |\xi_\infty|$ is given by the argument value at the center of the Sun, $\xi_\infty = (\Omega^2/\gamma K_x^2)\beta_0 e^{R_\odot/H}$. Notice that the width L depends significantly on the value of a central magnetic field via the parameter β_0 in Eq. (26).

The waves which are trapped within cavity loose wave energy due to partial absorption of their energy in the resonance Alfvén layer with the rate given by an imaginary part of the eigen frequency $\text{Im}(\omega) \neq 0$.

This dissipationless (i.e. reversible) damping is analogous to the collisionless mechanism of coherence losses for eigen (Alfvénic) modes considered in [30] for the Alfvén resonant layer which is the sheath of a solar coronal loop. The resonant absorption of Alfvénic surface waves leads to the heating of solar coronal loops. Moreover, the inertia of electrons $m_e \neq \infty$ ($v_{eT} = \sqrt{T/m_e} \neq 0$) should be taken into account or kinetic approach for wave-particle interaction is necessary to explain collisionless damping.

The same collisionless damping of MHD waves with absorption of waves in the Alfvén singular layer as a mechanism of heating of laboratory plasma was considered in [31] and in [32] - for heating of a nonuniform cosmic plasma.

In ideal MHD for a non-uniform medium one can also obtain the collisionless damping of eigen modes from the dispersion relation solving the corresponding eigen value problem with given boundary conditions[30].

There is another analogy that is well-known from plasma physics where the collisionless decrement of plasma waves comes both from dispersion relation for eigen modes and from the kinetic theory beyond the ideal MHD. The collisionless damping and increment are equal to each other for rates of the direct (inverse) Čerenkov emission (absorption) $e \leftrightarrow e\gamma$ in the wave-particle interaction.

The Landau damping of the Alfvén waves $\omega = k_x v_A(z_s)$ in the inverse Čerenkov process, $\gamma_A e \rightarrow e$, starts only within the Alfvén resonant layer $\xi = 1$ obeying the standard Čerenkov condition $\omega = \vec{k} \cdot \vec{v}_e$ where the electron velocity v_e is much bigger than the Alfvén one, $v_e \sim v_{eT} \gg v_A$. This means that those electrons which are moving almost across Alfvén layer (in ecliptic) could absorb Alfvén waves .

Thus, accounting for trapping of waves in the cavity $1 \leq \xi \leq \xi_\infty$ with partial losses of the wave energy within its upper boundary ($\xi = 1$) one can solve the problem of infinite wave amplitude at the resonance singular layer in framework of ideal MHD without taking into account of usual dissipation mechanisms (viscosity through collisions, ohmic dissipation,etc..). Really, for complex frequency the argument ξ becomes complex or the singularity $\xi = 1$ is removable (see below).

Our main task in present work is the derivation of *complex eigen frequencies and eigen functions* in a cavity we have considered. First step for that is the construction

of a common solution in the whole variable region $|\xi| < \infty$.

3.4.2 Common solution and continuity conditions

Let us assume that the complex frequency $\Omega = \Omega_1 + i\Omega_2 \equiv \Omega_1(1 + id)$ obeys the stability condition $\Omega_2 \leq 0$ ($\Omega_1^2 > \Omega_2^2$) and input the following notations for the independent variable $\xi = \xi_1 + i\xi_2 = \xi_1(1 + i\zeta)$:

$$\begin{aligned}\xi_1 &= \frac{\Omega_1^2 - \Omega_2^2}{\gamma K_x^2} \beta(z) = \frac{\Omega_1^2}{\gamma K_x^2} (1 - d^2) \beta(z) \\ \zeta &= \frac{\xi_2}{\xi_1} = \frac{2\Omega_1\Omega_2}{\Omega_1^2 - \Omega_2^2} = \frac{2d}{1 - d^2}.\end{aligned}\quad (30)$$

Notice that transition to free oscillations corresponds to the limit $d = \Omega_2/\Omega_1 \rightarrow 0$.

In the Fig. 1 we plot definition region for all three solutions upon the axis $\xi_1 = \operatorname{Re} \xi$ where the region $0 \leq \xi_1 \leq \xi_{1\infty}$ is the whole integration region. In common regions for overlap of solutions $u_{1,2,3}(\xi)$ we can use analytic continuation and connect these solutions each other.

By continuity of functions $u_{1,2,3}$ and of their derivatives $du_{1,2,3}/d\xi$ we choose two matching points in two overlap regions : (i) $\xi_1 = 1/2$ for the pair of solutions $u_3(\xi)$ and $u_2(\xi)$ and (ii) $\xi_1 = 3/2$ for the second pair $u_1(\xi)$ and $u_2(\xi)$. Then at these points we obtain the continuity conditions

$$\begin{aligned}u_3(\xi) &= u_2(\xi); \quad \frac{du_3(\xi)}{d\xi} = \frac{du_2(\xi)}{d\xi} \quad \text{for } \xi_1 = \frac{1}{2}, \\ u_1(\xi) &= u_2(\xi); \quad \frac{du_1(\xi)}{d\xi} = \frac{du_2(\xi)}{d\xi} \quad \text{for } \xi_1 = \frac{3}{2}.\end{aligned}\quad (31)$$

For the complex matching points chosen above,

$$\xi_0 = \frac{1}{2}(1 + i\zeta), \quad \xi_* = \frac{3}{2}(1 + i\zeta), \quad (32)$$

the arguments of functions in Eqs. (23), (28) are of the form

$$\begin{aligned}\Psi_0 &= \Psi|_{\xi_1=1/2} = 2\nu\sqrt{\xi_0 - 1}, \quad y_0 = y|_{\xi_1=1/2} = 2\nu\sqrt{-\xi_0}, \\ \Psi_* &= \Psi|_{\xi_1=3/2} = 2\nu\sqrt{3\xi_0 - 1}.\end{aligned}\quad (33)$$

Substituting the solutions $u_{1,2,3}$ and their derivatives $u'_{1,2,3}$ given by Eqs. (20), (21), (23), (25), (28), (29) into the continuity conditions Eq. (31) we obtain finally the system of algebraic transcendental equations

$$C_1 J_\mu(\Psi_0) + C_2 J_{-\mu}(\Psi_0) = D_1 J_{2K_\perp}(y_0),$$

$$\begin{aligned}
C_1 J'_\mu(\Psi_0) + C_2 J'_{-\mu}(\Psi_0) &= -D_1 \frac{\Psi_0}{y_0} J'_{2K_\perp}(y_0) , \\
C_1 J_\mu(\Psi_*) + C_2 J_{-\mu}(\Psi_*) &= \frac{1}{\sqrt{\xi_*}} (A_1 \xi_*^{i\nu} + A_2 \xi_*^{-i\nu}) , \\
C_1 J'_\mu(\Psi_*) + C_2 J'_{-\mu}(\Psi_*) &= \frac{i\Psi_*}{2\nu \xi_* \sqrt{\xi_*}} (A_1 \xi_*^{i\nu} - A_2 \xi_*^{-i\nu}) ,
\end{aligned} \tag{34}$$

from which we can define all arbitrary constants except of one, for instance, we choose $D_1 \neq 0$. Let us recall that in the solution near surface of the Sun in Eq. (28) we used the boundary condition $D_2 = 0$ excluding irregular part of solution.

Notice that in low frequency approximation $\Omega \ll 1$ the index ν is large, $|\nu| \gg 1$ (see Eq. (20)), resulting in large arguments of Bessel functions: $|\Psi_*| > |\Psi_0| \gg 1$, $|y_0| \gg 1$. As result we substitute Bessel functions by their asymptotical expansions for large arguments.

3.4.3 Dispersion equation and spectrum of MAG waves

Let us turn to the boundary condition at the center of the Sun, $v_z|_{z=R_\odot} = 0$. From the Eq. (10) in the limit $|\xi| \gg 1$ we obtain the ratio for coefficients $A_{1,2}$ in the solution Eq. (20) for central region of the Sun:

$$\frac{A_1}{A_2} = -\xi_\infty^{-2i\nu} . \tag{35}$$

Thus, using the last ratio and the system Eq. (34), we obtain the dispersion equation for the MAG waves in the Sun:

$$\frac{\Psi_*}{2\nu \xi_*} \frac{(\varepsilon - 1)}{(\varepsilon + 1)} = 1 , \tag{36}$$

where the complex parameter $\varepsilon = \varepsilon_1 + i\varepsilon_2 = -(\xi_*/\xi_\infty)^{2i\nu}$ can be expressed for small damping decrement ($d^2 \ll 1$) via real functions

$$\varepsilon_1 = -e^{d\Phi} \cos \Phi , \quad \varepsilon_2 = -e^{d\Phi} \sin \Phi . \tag{37}$$

Here the parameter $\Phi = \Phi(\Omega_1, k_\perp, \alpha, B_0)$ depends on the *real part* of the eigen frequency Ω_1 :

$$\Phi = 2\nu_* \ln \left(\frac{3\gamma K_x^2}{2\Omega_1^2 \beta_0} e^{-R_\odot/H} \right) , \tag{38}$$

where $\nu_* = \text{Re } (\nu) = \sqrt{(\gamma - 1)/\gamma} (K_\perp/\Omega_1)$ is the real part of the index ν ; $\tan \alpha = K_y/K_x$ is different from zero for oblique wave propagation, $K_y \neq 0$.

As result of the parametrization $\varepsilon_{1,2}(d, \Omega_1)$ in Eq. (37) the dispersion equation Eq.(36) can be rewritten as the system of transcendental equations for the real (Ω_1)

and the imaginary (d) parts of eigen frequency

$$\begin{aligned} d(\varepsilon_1 - 1) + \varepsilon_2 \left(1 - \frac{3}{\sqrt{2}}\right) &= 0, \\ d\varepsilon_2 + 1 - \varepsilon_1 + \frac{3}{\sqrt{2}}(1 + \varepsilon_1) &= 0. \end{aligned} \quad (39)$$

One can easily see that $d = 0$ is not a solution of Eq. (39). This means that full reflection from resonance layer never happens. Accounting for notations in Eq. (37) we obtain from Eq. (39) another form of dispersion equations

$$\begin{aligned} \Phi \tan \Phi &= \frac{6\sqrt{2}}{7} \ln \frac{7}{11 - 6\sqrt{2}}, \\ d &= \frac{1}{\Phi} \ln \frac{7}{11 - 6\sqrt{2}}, \end{aligned} \quad (40)$$

where Φ is given by Eq. (38).

Since a solution of the first equation in Eq. (40) depends on the harmonic number $n = 1, 2, \dots$ only, $\Phi = \Phi(n)$, the damping decrement d depends on that harmonic number too, $d = d(n)$. This dependence is plotted in Fig. 2. The calculation gives $d < 0$ for positive values $n \geq 1$. One can see from Fig. 2 that number of harmonics is finite: $1 \leq n \leq n_{max}$. While $|d|$ is small for a large n the nonzero value $d \neq 0$ for n_{max} means that energy losses in cavity always happen due to resonance absorption.

The phase velocity of waves along the magnetic field \vec{B}_0 normalized to the sound velocity $V_{ph}/c_s = \omega_1/k_x c_s = \Omega_1/\sqrt{\gamma} K_x$ is the second solution of dispersion equations Eq. (40) as it follows from the definition of the function Φ in Eq. (38). This solution depends on all set of parameters: the harmonic number n , the value of magnetic field B_0 , the wave angle of incidence α , $\tan \alpha = k_y/k_x$, the adiabatic parameter γ and the wave number k_x . In Fig. 3a we show the dependence $V_{ph}(n)$ on n for different values of the magnetic field B_0 and for a particular case of the longitudinal wave propagation, $\vec{k} \parallel \vec{B}_0$, $k_y = 0$.

For a given n the dispersion equation has two solutions: the high frequency one (plotted by the solid line in Fig. 3a) and the low frequency one (dashed line). The cross point of these curves determines the maximal value n_{max} . The value n_{max} decreases when the magnetic field B_0 increases. The analogous dependence $\omega_1(n)$ for the fixed magnetic field value 10 G and for different wave propagation angles ($k_\perp/k_x = 1, 2, 5$ corresponds to $\alpha = 0^\circ, 60^\circ, 78^\circ$) are shown in Fig. 3b. The node number n increases with increase of α .

The change of a node number n in dependence on B_0 , α is connected with the change of a cavity width for these varying parameters. Combining results in Figs. 2,3 we can find the imaginary part of the eigen frequency $\Omega = \Omega_1 + i\Omega_2$, $\Omega_2(n) = d\Omega_1$, for a given harmonic n .

The peculiarities of the eigen modes $\omega_1(n, B_0, k_x, \alpha)$ are seen from Figs. 3a, 3b: the high frequency branch (solid lines) has the minimum value $\omega_{min}^{(high)}(n_{max})$ for n_{max}

and the maximum one $\omega_{max}^{(high)}(n = 1)$ for $n = 1$. Vice versa, the low frequency branch (dashed lines) has the minimal value $\omega_{min}^{(low)}(n = 1)$ for $n = 1$ and the maximal one $\omega_{max}^{(low)}(n_{max})$ for $n = n_{max}$. Note that the first harmonic ($n = 1$) for the high frequency branch corresponds to the magnetosonic waves: $V_{ph} \sim c_s$ that is outside of our approximation of low frequencies, $\omega \ll k_x c_s$. As a result we got too fast damping of such waves, $|d| \gtrsim 10^{-2}$.

We do not consider here the low frequency branches (dashed lines) for which the rotation of the Sun becomes important. This rotation changes crucially properties and spectra of low frequency oscillations ($T \geq T_\odot$) in the Sun as it was found in [33].

Note that since a node number $1 \leq n \leq n_{max}$ is finite a continuum does not arise, spectrum is always discrete (ridge structure).

The spectrum $f = \omega_1(n, B_0, k_x, \alpha = 0)/2\pi$ (in the dimension units μHz) is shown in Fig. 4 for the longitudinal wave propagation: we plotted the real part of frequencies $\omega_1(n, B_0 = 10 G, k_x)$ in dependence on the wave number $k_x R_\odot$ for the particular case $B_0 = 10 G$, for $k_y = 0$ and for different harmonics $1 \leq n \leq n_{max} = 2780$. The curve $n = 2780$ is common for low and high frequency branches. Since the long period $f^{-1} = (1 \mu Hz)^{-1} = 11,6 \text{ days}$ is at the boundary of our approach we conclude that all dashed lines in Fig. 4 with $n \leq n_{max} = 2780$ and some part of solid lines ($n \gtrsim 2000$, or $f \lesssim 1 \mu Hz$) correspond to too low frequencies when we need to take into account the Sun rotation (with the period $T_\odot \simeq 27 \text{ days}$).

4 The position z_s and the width Δz_s of a resonant layer

The appearance of a resonant Alfvén layer within the Sun, $0 \leq z_s \leq R_\odot$ can lead to an interesting application for SNP. From the condition $\xi_1 = 1$ substituted into Eq. (30) we have found the distance of a singular layer from the center of the Sun for the case $d \ll 1$:

$$\frac{z_s}{R_\odot} = 1 - \frac{z_{1s}}{R_\odot} = 1 - \frac{1}{10} \ln\left(\frac{\gamma K_x^2}{\beta_0 \Omega_1^2}\right) = 1 - \frac{1}{10} \ln\left(\frac{c_s^2}{\beta_0 v_{ph}^2}\right), \quad (41)$$

where z_{1s} is the distance of the same singular point measured from the surface at $z = 0$. In Fig. 5 (a,b) we show the harmonic number dependence $z_s(n)$ for given values of the magnetic field B_0 and the wave incidence angle α .

One can see that for any values of the parameters B_0 , α and for the low frequency branch (dashed curves) the resonant layer is near the center of the Sun ($z_s/R_\odot \leq 0.25$). For the high frequency branch (solid curve) it occurs at the edge of the solar core relevant to the MSW resonance region and either in the radiative zone or in the convective one ($0.25 \leq z_s/R_\odot \leq 1$). With increase of the magnetic field B_0 the acceptable node number $n \leq n_{max}$ decreases (see Fig. 5a for fixed $k_y = \alpha = 0$) while for the fixed magnetic field value $B_0 = 10 G$ it increases if α increases (Fig. 5b).

Let us turn to the derivation of the resonant layer width Δz_s where a significant part of the wave energy is concentrated. For this goal we have calculated the density of the hydrodynamical energy flux across an Alfvén resonant layer

$$P_z^{(mech)}(\xi_1(z)) = \frac{1}{2} \text{Re}(\delta p \bar{v}_z^*) = \frac{p_0}{2} \text{Re} \left[\frac{v_z^*}{i\omega} \left(\frac{v_z}{H} + \gamma u \right) \right], \quad (42)$$

where the pressure perturbation $\delta p = (p_0/i\omega)(v_z/H + \gamma u)$ is obtained from the system Eq. (7), v_z^* is the complex conjugate value of v_z and the function $u(z) = u_2(z)$ is given by the Eq. (23).

Notice that we have neglected electromagnetic energy flux density of waves across resonant layer because near that Alfvén layer ($\xi \sim 1$) the z-component of the Poynting vector is much smaller than the mechanical one, $P_z^{(em)} \ll P_z^{(mech)}$, since the condition $p_{\text{gas}} \gg p_{\text{mag}}$ is fulfilled within the Sun.

In the case of free oscillations the imaginary part of the eigen frequency is zero, $\Omega_2 = d = 0$, and the flux $P_z^{(mech)}(\xi)$ is infinite at the singular layer, $P_z^{(mech)}(\xi = 1) = \infty$. However, for eigen modes bounded within cavity ($d \neq 0$) this flux is finite, $P_z^{(mech)}(\xi_1 = 1) \neq \infty$, and the function $P_z^{(mech)}(\xi)$ has a finite maximum for the argument $\xi_1 = 1$.

The height of this peak is determined by the value of $d = \Omega_2/\Omega_1$. In order to find the half-width of that peak we have used the equation $P_z^{(mech)}(\xi_1(z)) = P_z^{(mech)}(\xi_1 = 1)/2$ which has two solutions: $\xi_1^- < 1$ and $\xi_1^+ > 1$.

For the half-width we have found

$$\Delta z_s = H \ln \frac{\xi_1^+}{\xi_1^-}. \quad (43)$$

In Fig. 6 we show the dependence of the width Δz_s on node numbers n for different values of the background magnetic field B_0 and for the longitudinal wave propagation, $k_y = 0$. One can see that the width Δz_s becomes more narrower for large node numbers lowering to $\Delta z_s \lesssim 1 \text{ km}$ for the case $B_0 = 10 \text{ G}$ in the region $n \geq 1000$ (radiative zone, see Fig. 5a where the corresponding position $z_s(n)$ is shown).

We have found too narrow spikes (hundreds meters) near the node number $n \sim 2680$ in the most interesting region $z = r_{MSW} \sim 0.3R_\odot$ for the same ambient magnetic field $B_0 = 10 \text{ G}$ while for the field $B_0 = 100 \text{ G}$ the width reaches $\Delta z_s \sim 5 \text{ km}$ for the same position z_s with the node number $n \sim 268$ (compare Figs. 7a, 7b below).

In reality the position $z_s(n)$ is discrete in dependence on the node number n (it looks continuous in large-scale Figs. 5a, 5b). For the high frequency branch for which our approximation of the Sun at rest seems to be valid we have shown in Figs. 7a, 7b (for the background magnetic field $B_0 = 10 \text{ G}$ and $B_0 = 100 \text{ G}$ correspondingly) the distance between neighbouring resonant Alfvén layers for the most interesting region near the MSW resonant point ($r_{MSW} \sim 0.3R_\odot$). One can see that the distance between layers n and $n + 1$ is changing in order of magnitude from $z_s(n) - z_s(n + 1) \simeq 200 \text{ km}$ ($B = 10 \text{ G}$) up to $z_s(n) - z_s(n + 1) \simeq 2000 \text{ km}$ ($B = 100 \text{ G}$).

5 Density fluctuations

Considering whole solar interior $0 < z < R_{\odot}$ for the same background magnetic field values $B = 10$ G and $B = 100$ G we have found many resonant layers shown in our main Figures 8a, 8b where an unnormalized density fluctuation $\delta\rho(z)/\rho$ (calculated from Eq. (11)) is plotted as the function of z , $0 \leq z \leq R_{\odot}$.

Notice that a height of spikes occurs the random one because of uncertainty of numerical calculation near each resonant layer when the numerical code is running along whole solar radius with many spikes skipping occasionally some sharp maxima.

Obviously from comparison of Figs. 8a, 8b that in the case of the small magnetic field $B_0 = 10$ G spikes are placed more tightly than in the case of $B_0 = 100$ G and really resemble a density matter noise since small distance between neighbouring resonant layers shown in Fig. 7a,b.

Let us estimate the enhancement of the density perturbation $\delta\rho/\rho_0$ given by Eq. (11),

$$A = \frac{\delta\rho/\rho_0)_{z=z_s}}{(\delta\rho/\rho_0)_z} \simeq \frac{|v_z(\xi)/H + u_2(\xi)|_{z=z_{1s}}}{|v_z(\xi)/H + u_2(\xi)|_z}, \quad (44)$$

in the vicinity of an Alfvén resonant layer, $z - z_{1s} \ll H$, obeying the inequalities

$$(\xi_1 - 1) \ll \frac{v_A^2}{c_s^2} = (\beta_0 e^{z/H})^{-1} \ll 1,$$

where the real part of the ξ -argument equals to $\xi_1 = e^{(z-z_{1s})/H}$ (here $\xi_1 > 1$ since $z > z_{1s}$) and the first inequality means a finite small displacement from the resonant point z_{1s} provided the large parameter $\beta_0 = 4 \times 10^4 \gg 1$ for the small magnetic field value $B_0 = 10$ G is substituted.

For simplicity let us also consider the longitudinal wave propagation $\vec{k} \parallel \vec{B}_0$, $k_y = 0$, when the index μ is real, or for hydrogen with $\gamma = 5/3$ we find $\mu = 2\sqrt{(\gamma-1)/\gamma} \sim 1.27$.

One can easily check from Eq. (10) that for conditions chosen above the longitudinal speed component is of the order

$$v_z(\xi)/H \approx -\gamma u_2(\xi) + O(\beta_0^{-1}), \quad (45)$$

where the singular solution $u_2(\xi)$ in Eq. (23) takes of the asymptotic form $u_2(\xi) \simeq C_2 J_{-\mu}(\Psi) \approx C_2 (\nu \sqrt{\xi - 1})^{-\mu} / \Gamma(\mu + 1)$.

Thus, the amplification Eq. (44) of a MAG wave density amplitude $\delta\rho/\rho_0$ is given by

$$A \simeq \left[\frac{((z - z_{1s}(n))/H)^2 + 4d^2(n)}{4d^2(n)} \right]^{1+\mu/4}, \quad (46)$$

or enhancement is really big because of transparency for MAG eigen waves shown in Fig. 2, $d(n) = \Omega_2/\Omega_1 \ll 1$, especially for large harmonics $n \gg 1$.

In Figs. 9a,b we have shown the profile $\delta\rho_n(z)/\rho_0$ of the selected mode $n = 300$ built numerically in the idealized case $B_0 = 10 G$ and $k_y = 0$ for which the resonant layer position occurs just under the top of the convective zone, $z_s/R_\odot = 1 - z_{1s}/R_\odot = 0.9985$ (in our model we neglect turbulent properties of medium in that region).

One can easily understand the continuous exponential increase of the wave $n = 300$ propagating from the center $z = R_\odot$ up the resonant Alfvén layer $z_{1s} \sim 0.01$ near the photosphere (see Fig. 9b). This follows from the solution Eq. (20) extended on whole solar interior and rewritten as $u_1(z) = e^{-z/2H}(A_{10}e^{iz\sqrt{b}/H} + A_{20}e^{-iz\sqrt{b}/H})$.

For this largest cavity the wave length of MAG waves along z-axis equals to $\lambda_z \sim z_s/300 \sim 2300 km$ and the enhancement seen from Fig. 9a (for unnormalized amplitude) is of a few orders of magnitude ($A \sim 10^2 - 10^3$ for the distance $\lambda_z \sim (z - z_{1s})$) in good agreement with the analytic estimate Eq. (46).

From the right side of that resonant layer one can see in Fig. 9a a steep decrease of density perturbation described by Eq. (11) through the solution Eq. (28) vanishing exponentially to the surface $z = 0$.

6 Discussion

We have studied MHD (or more correct name: MAG) wave origin of the solar matter density fluctuations $\delta\rho/\rho_0$ that could be important both for Solar Physics and for the MSW solution to SNP.

We have found MAG-wave eigen modes for cavities within solar interior with the spectrum given by the dispersion equations Eq. (40). The lower boundary of cavities is the common point - center of the Sun, $z = R_\odot$, where the longitudinal perturbations are absent, $v_z = b_z = 0$, and the top (upper) boundary is given by the Alfvén resonant layer position, $z = z_s(n)$, that depends on the node number n , the background magnetic field value B_0 and the wave numbers k_x, k_y .

A finite amplitude of the density perturbation $\delta\rho/\rho$ in each Alfvén resonant layer is determined by the mechanism like the collisionless damping of MAG waves that is similar with the Landau damping of Alfvén waves = absorption by electrons at the Čerenkov resonance $\omega = k_x v_A = k v_e \cos\theta$, $v_e \gg v_A \sim 1 cm/s$, $\theta \sim \pi/2$. Thus, electrons moving almost across Alfvénic layer can absorb these waves.

Crucial and open questions for future exploration are:

- How to enhance MAG eigen modes existing at a negligible fluctuation level within cavities deep under bottom of the convective zone and where is the energy source for an amplification of MAG waves in solar interior? What is the normalization of MAG eigen modes? Full set of ortonormalized functions (like in SHM) is still not built for these MAG waves.
- Does the dispersion relation that could be obtained via a solution of kinetic equations in inhomogeneous magnetised plasma coincide with the dispersion found from Eq. (40) in the MHD boundary problem?

c) Can we apply the simplest analysis given here to another geometry of the background magnetic field \vec{B}_0 , how to generalize the analytic approach developed in present work in the case of a non-uniform magnetic field $\vec{B}_0(z)$ and how to take off the isothermal approximation $T_0 = \text{const}$? Latter step would allow us to construct the sound speed profile $c_s(z)$ connected with the inverse problem like in SHM.

As the necessary step for a generalization and for the checking of the simple asymptotic solution found here an independent numerical solution of the same initial Heun equation Eq. (15) or even of the whole MHD equation system Eq. (7) is needed to confirm, first, the presence of spikes shown in our Figs. 8a, 8b.

An answer on the first question relies on the excitation of a contour through the connection (via a non-linear interaction) with the second (neighbouring) contour excited by the given generator. In the oscillation theory some mechanisms for energy transfer in two- or n-contour systems are well-known. They are based on solutions of the telegraph equation in electrodynamics for two (or n-cell) connected contours or of the non-linear oscillator equations for two (n-cell) connected pendulums in mechanics.

The key question whether the energy transfer time would be shorter than the collisionless damping time of eigen modes in neighbouring contours has a promising solution for high harmonics $n \gg 1$ for which the temporal damping occurs small in our model, $d(n) \ll 1$.

The non-linear interaction in hydrodynamics is given by the $\vec{v}\nabla\vec{v}$ -term that was omitted in the linear theory. This term can lead to an amplification of the mode v_1 if the second mode v_2 (excited in a contour displaced in space with respect to the first one) was generated by an external source. On this way one can imagine a turbulent source in the convective zone (with a spectrum including low frequencies in our model (*a few days*) $^{-1}$) with the continuous transfer of energy down the bottom of the convective zone.

One can not exclude also another energy source connected with radiative losses and due to some spatial inhomogeneities of thermonuclear reactions in central region or a diffusion there (for instance due to ^3He diffusion near $r \sim 0.2R_\odot$). In that case a source Q = the rate of all energy density sources and losses arises in the r.h.s. of the energy conservation law Eq. (5).

To judge of whether MHD regular waves may be a plausible source of matter noise let us note how they can be converted to a noise. Even infinite sum over eigen-values (radial numbers $n = 0, 1..$ and angular moments l) does not lead to the noise as it is argued in [22] for g-modes in SHM.

The presence of regular waves with a small wave length is only a *motivation* but not *realization* of the white noise. Really an instability (like buoyance force disappearance at the bottom of the convective zone as a source of acoustic turbulence there) can lead to the white noise with continuous spectrum due cascade or inverse cascade processes with *any change of the turbulence scale*. This is the *non-linear* process with the decay (or fusion) of regular modes (of number 1 and number 2) obeying the conservation laws: $\omega = \omega_1 + \omega_2$, $\vec{k} = \vec{k}_1 + \vec{k}_2$. In hydrodynamics or in MHD this corresponds to

the non-linear term $(\vec{v}\nabla)\vec{v}$ omitted in linear approximation in SHM ($B_0 = 0$) and in linear MHD.

Thus, without any assumption about a neutrino magnetic moment we have proposed a way to modify the MSW solution to SNP. The registration of 1-10 days variations of solar neutrino flux in underground detectors with large statistics of neutrino events seems to be a signature of MHD wave influence. The search of Day/Night (D/N) variations due to Earth effects for neutrino oscillations has been already carried out in the SuperKamiokande (SK) experiment to check the MSW scenario. It seems to be not difficult to recognize a few days periods from the Fourier analysis of the SK data if MAG wave density perturbations would occur large enough (!?).

Acknowledgements

The authors thank Cliff Burgess, Alexander Rez, Jose Valle and especially Alexei Bykov for fruitful discussions. This work has been supported by RFFR grants 97-02-16501, 98-02-17062 and by INTAS grant 96-0659 of the European Union.

References

- [1] K. Lande (Homestake Collaboration) in *Neutrino '98*, Proceedings of the XVIII International Conference on Neutrino Physics and Astrophysics, Takayama, Japan, 4-9 June 1998, edited by Y. Suzuki and Y. Totsuka, to be published in Nucl. Phys. B (Proc. Suppl.).
- [2] Y. Fukuda et al. (Kamiokande Collaboration), Phys. Rev. Lett. 77 (1996) 1683.
- [3] V. Gavrin (SAGE Collaboration) in Neutrino '98 [1].
- [4] T. Kirsten (GALLEX Collaboration) in Neutrino '98 [1].
- [5] Y. Suzuki (SuperKamiokande Collaboration) in Neutrino '98 [1].
- [6] J.N. Bahcall, S. Basu, M.H. Pinsonneault, Phys. Lett. B433 (1998) 1.
- [7] V. Castellani, S. Degl'Innocenti, G. Fiorentini, Astron. Astrophys. 271 (1993) 601.
- [8] V. Berezinsky, astro-ph/9710126, invited lecture at 25th International Cosmic Ray Conference, Durban, 28 July - 8 August, 1997.
- [9] V.N. Gribov, B.M. Pontecorvo, Phys. Lett. B28 (1969) 493.
- [10] S.P. Mikheev, A.Yu. Smirnov, Sov. J. Nucl. Phys. 42 (1985) 913; Nuovo Cimento C9 (1986) 17; L. Wolfenstein, Phys. Rev. D17 (1978) 2369.

- [11] C.S. Lim, W.J. Marciano, Phys. Rev. D37 (1988) 1368; E.Kh. Akhmedov, Sov. J. Nucl. Phys. 48 (1988) 382; Phys. Lett. B213 (1988) 64.
- [12] W.A. Dziembowski, Bull. Astron. Soc. India 24 (1996) 133; S. Degl'Innocenti, W.A. Dziembowski, G. Fiorentini, B. Ricci, Astropart. Phys. 7 (1997) 77.
- [13] E.N. Parker, *Cosmical magnetic fields*, Clarendon Press, Oxford, 1979; V.A. Kutyvitskii and L.S. Solov'ev, Sov. Phys. JETP, 78 (1994) 456.
- [14] V. Semikoz, J.W.F. Valle, Nucl. Phys. B425 (1994) 651; erratum Nucl. Phys. B485 (1997) 545 [hep-ph/9607208];
S. Sahu, V. Semikoz and J.W.F. Valle, hep-ph/9512390;
P. Elmforss, D. Grasso and G. Raffelt, Nucl. Phys. B479 (1996) 3;
J.C.D'Olivo, J.Nieves, Phys. Lett. B383 (1996) 87;
- [15] H. Nunokawa, V.B. Semikoz, A.Yu. Smirnov, J.W.F. Valle, Nucl. Phys. B501 (1997) 17-40, e-print Archive: hep-ph/9701420.
- [16] A. Kuzenko and G. Segre, Phys. Rev. Lett. 77 (1996) 4872.
- [17] N. Boruta, Ap. J. 458 (1996) 832.
- [18] John N. Bahcall, *Neutrino Astrophysics*, Cambridge University Press, 1988.
- [19] P.I. Krastev, A.Yu. Smirnov, Phys. Lett. B 338 (1989) 341; Mod. Phys. Lett. A 6 (1991) 1001.
- [20] A. Schafer, S.E. Koonin, Phys. Lett. B185 (1987) 417;
R.F. Sawyer, Phys. Rev. D 42 (1990) 3908; A. Abada, S.T. Petcov, Phys. Lett. B 279 (1992) 153.
- [21] H. Nunokawa, A. Rossi, V.B. Semikoz and J.W.F. Valle, NPB 472 (1996) 495.
- [22] P. Bamert, C.P. Burgess and D. Michaud, *Neutrino Propagation Through Heliosesmic Waves*, Preprint McGill-97/13, hep-ph/9707542;
C.P. Burgess, D. Michaud, Ann. Phys., (NY) 256 (1997) 1.
- [23] F.N. Loret, A.B. Balantekin, Phys. Rev. D50 (1994) 4762.
- [24] Yu.D. Zhugzhda, N.S. Dzhalilov, Geophys. Astrophys. Fluid. Dynamics, 35 (1986) 131.
- [25] M.M. Guzzo, N. Reggiani and J.N. Colonia, Phys. Rev. D56 (1997) 588.
- [26] M. Stix, *The Sun*, Springer-Verlag (Berlin, New York, London, Paris, Tokio) 1989, 890 pp.

- [27] N.S. Dzhailov, Yu.D. Zhugzhda, Astron. Zh., 67 (1990) 561 (in Russian, translated to English).
- [28] K. Heun, Math. Ann. 33 (1889) 161-179.
- [29] E.R. Priest, *Solar Magnetohydrodynamics*, by D. Reidel Publishing Company, Dordrecht, Netherlands, 1982.
- [30] J. Ionson, Ap. J. 226 (1978) 650; 254 (1982) 318; 276 (1984) 357; J.V. Hollweg, Ap. J. 312 (1987) 880; 320 (1987) 875.
- [31] A. Hasegawa, C. Uberoi, *The Alfvén wave*, Washington D.C., Technical Inform. Center, UUS Depart. of Energy, 1988.
- [32] L. Nocera, B. Leroy, E.R. Priest, Astron. Astrophys., 133 (1984) 387.
- [33] V.N. Oraevsky, N.S. Dzhailov, Astron. Zh. 74 (1997) 99 (in Russian); Translated in: V.N. Oraevskii, N.S. Dzhailov, Astronomy Reports, 41 (1997) 91.

Figure Captions

Fig. 1 The integration region $0 \leq \xi_1 = \text{Re } \xi \leq \xi_{1\infty}$ for all three asymptotic solutions (downwards- to the center of the Sun). Here $\xi_1 = 1/2$ is the matching point for the solutions $u_2(\xi)$ and $u_3(\xi)$ and $\xi = 3/2$ is the matching point for $u_1(\xi)$ and $u_2(\xi)$

Fig. 2. The ratio of imaginary and real parts of the eigen frequencies $d = |\Omega_2| / \Omega_1$ in dependence on the node number n

Fig. 3a and b. The normalized phase velocity $v_{ph}/c_s = v_A/c_s$ in dependence on the node number n : **a** for the longitudinal wave propagation $k_y = 0$ and for different values of the ambient magnetic field B_0 (in Gauss), **b** for the fixed $B_0 = 10$ G and for different angles of the wave propagation $k_\perp/k_x = 1/\cos\alpha = 1, 2, 3, 5$. The low (dashed) and high (solid) frequency branches matched at n_{max} are plotted

Fig. 4. The spectrum $f = \omega_1(n, B_0, k_x)/2\pi$ for the longitudinal wave propagation ($k_y = 0$). The ambient magnetic field $B_0 = 10$ G is chosen. The low frequency branches (dashed lines) and the high frequency ones (solid lines) matched at $n_{max} = 2780$ are plotted for different node numbers n . For short wave lengths $\lambda_x = 2\pi/k_x$ the characteristic periods of MAG waves $T = f^{-1} = (1 \div 10 \mu\text{Hz})^{-1} = 11.57 \div 1.157 \text{ days}$ correspond to the node numbers $n = 300 \div 2000$

Fig. 5a and b. The Alfvén layer position $z_s(n)$: **a** for the longitudinal wave propagation $k_y = 0$ in dependence on node numbers n for the ambient magnetic field values $B_0 = 10 \div 100$ G, **b** for the fixed background field $B_0 = 10$ G in dependence on the wave propagation angles, $(\cos\alpha)^{-1} = k_\perp/k_x = 1, 2, 3, 5$. Dashed curves respond to too low frequency branches $T = f^{-1} \geq T_\odot$ beyond the approximation of the Sun at rest, $T \ll T_\odot = 27 \text{ days}$

Fig. 6. The width $\Delta z_s(n)$ of Alfvén resonant layers for the longitudinal wave propagation $k_y = 0$ in dependence on the node number n for the ambient magnetic field values $B_0 = 10, 20, 100$ G

Fig. 7a and b. The positions $z_s(n)$ for Alfvén layers near the MSW resonant region $z_{MSW} \approx 0.3R_\odot$ for the ambient magnetic field: **a** $B_0 = 10$ G (the distance between neibouring layers equals to $z_s(n-1) - z_s(n) \sim 200 \text{ km}$), **b** $B_0 = 100$ G (the distance between neibouring layers equals to $z_s(n-1) - z_s(n) \approx 2000 \text{ km}$)

Fig. 8a and b. The density profile $\delta\rho(z)/\rho_0(z)$ in the case of longitudinal wave propagation $k_y = 0$. The spikes (with unnormalized amplitudes) respond to Alfvén resonant layers with the node numbers: **a** for the ambient magnetic field $B_0 = 10$ G from $n \sim 300$ near the photosphere $z_s = R_\odot$ up $n = 2680$ at the MSW region $z_s = 0.3R_\odot$, **b** for the ambient (large-scale) field $B_0 = 100$ G from $n \sim \text{tens}$ at the photosphere $z_s = R_\odot$ up $n = 268$ at the MSW resonant point $z_{MSW} = 0.3R_\odot$. Small amplitudes of regular MAG waves that fill each cavity from the center of the Sun up the corresponding right boundary $z_s(n)$ (up a spike) are not seen between spikes while really the wave length within an inner cavity, $\lambda_z = 2\pi/k_z = z_s/n$, is very short since $n \gg 1$

Fig. 9a and b. The density perturbation profile $\delta\rho_n(z)/\rho_0$ for the wave mode

$n = 300$ in the background field $B_0 = 10$ G: **a** small-scale structure of the density perturbation mode $n = 300$ near the resonant layer position $z_s/R_\odot = 0.9985$, **b** the same density perturbation mode within the largest cavity with the upper bound near the photosphere, $z_s/R_\odot \sim 0.99$ (not seen on the large scale $0 \leq z \leq R_\odot$),

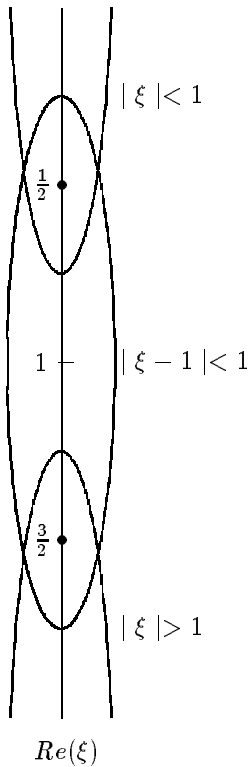


Fig. 1. The integration region $0 \leq \xi_1 = \operatorname{Re} \xi \leq \xi_{1\infty}$ for all three asymptotic solutions (downwards- to the center of the Sun). Here $\xi_1 = 1/2$ is the matching point for the solutions $u_2(\xi)$ and $u_3(\xi)$ and $\xi = 3/2$ is the matching point for $u_1(\xi)$ and $u_2(\xi)$.

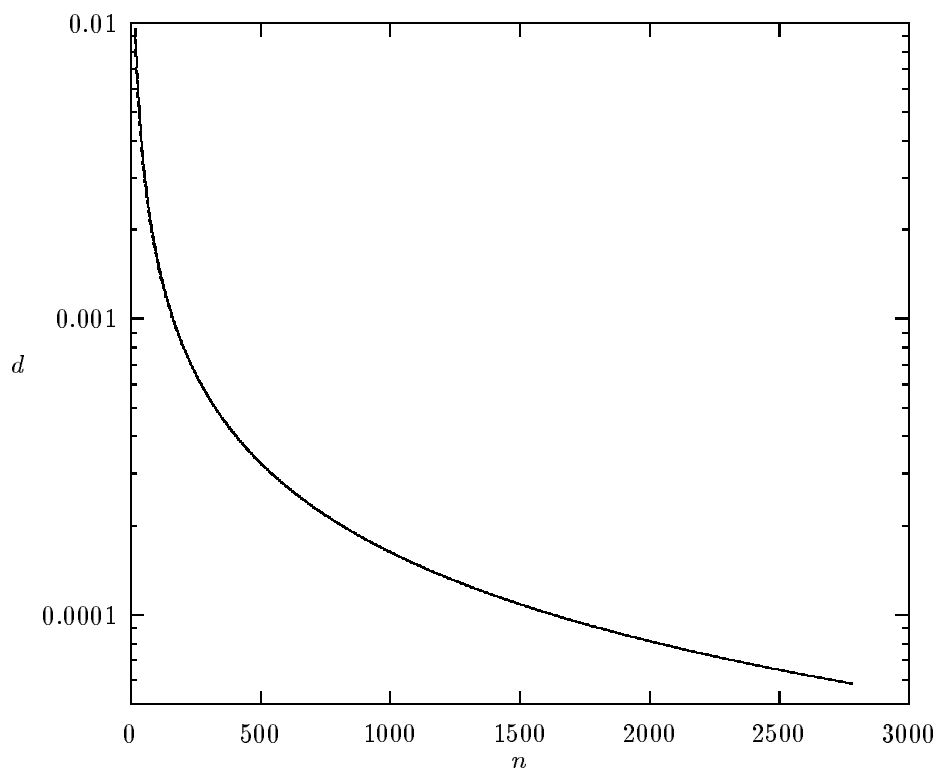


Fig. 2. The ratio of imaginary and real parts of the eigen frequencies $d = \Omega_2/\Omega_1$ in dependence on the node number n .

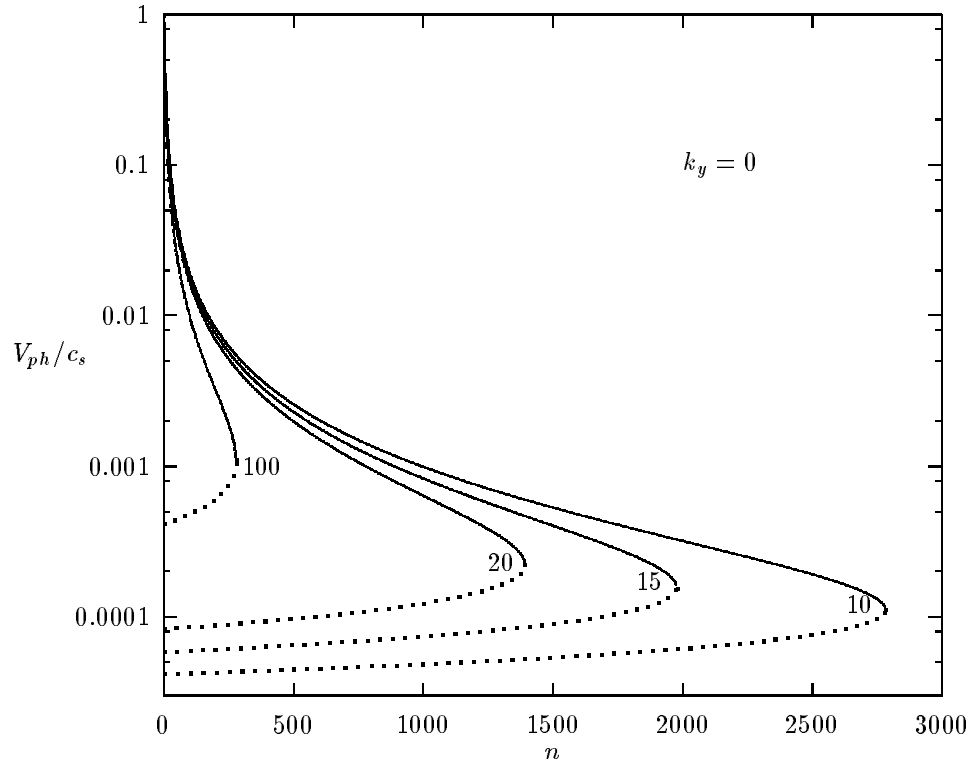


Fig. 3a. The normalized phase velocity V_{ph}/c_s in dependence on the node number n for the longitudinal wave propagation $k_y = 0$ and for different values of the ambient magnetic field B_0 (in Gauss). The low (dashed) and high (solid) frequency branches matched at n_{max} are plotted.

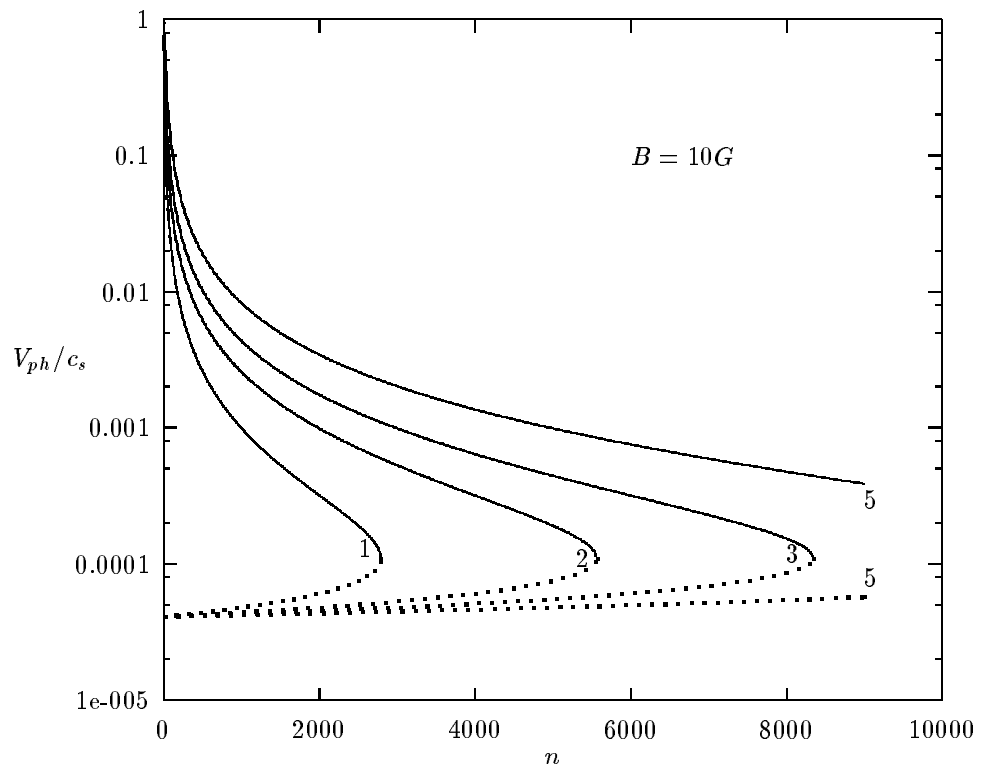


Fig. 3b. The normalized phase velocity V_{ph}/c_s in dependence on the node number n for the fixed $B_0 = 10$ G and for different angles of the wave propagation $k_{\perp}/k_x = 1/\cos \alpha = 1, 2, 3, 5$.

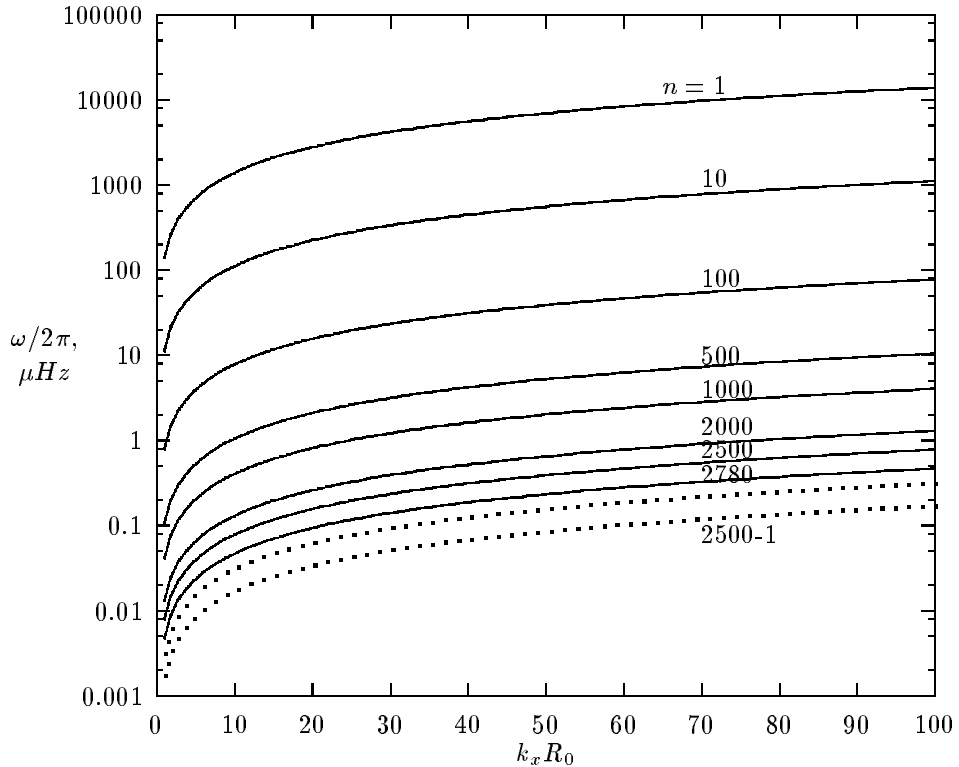


Fig. 4. The spectrum $f = \omega_1(n, B_0, k_x)/2\pi$ for the longitudinal wave propagation ($k_y = 0$). The ambient magnetic field $B_0 = 10$ G is chosen. The low frequency branches (dashed lines) and the high frequency ones (solid lines) matched at $n_{max} = 2780$ are plotted for different node numbers n . For short wave lengths $\lambda_x = 2\pi/k_x$ the characteristic periods of MAG waves $T = f^{-1} = (1 \div 10 \mu\text{Hz})^{-1} = 11.57 \div 1.157 \text{ days}$ correspond to the node numbers $n = 300 \div 2000$.

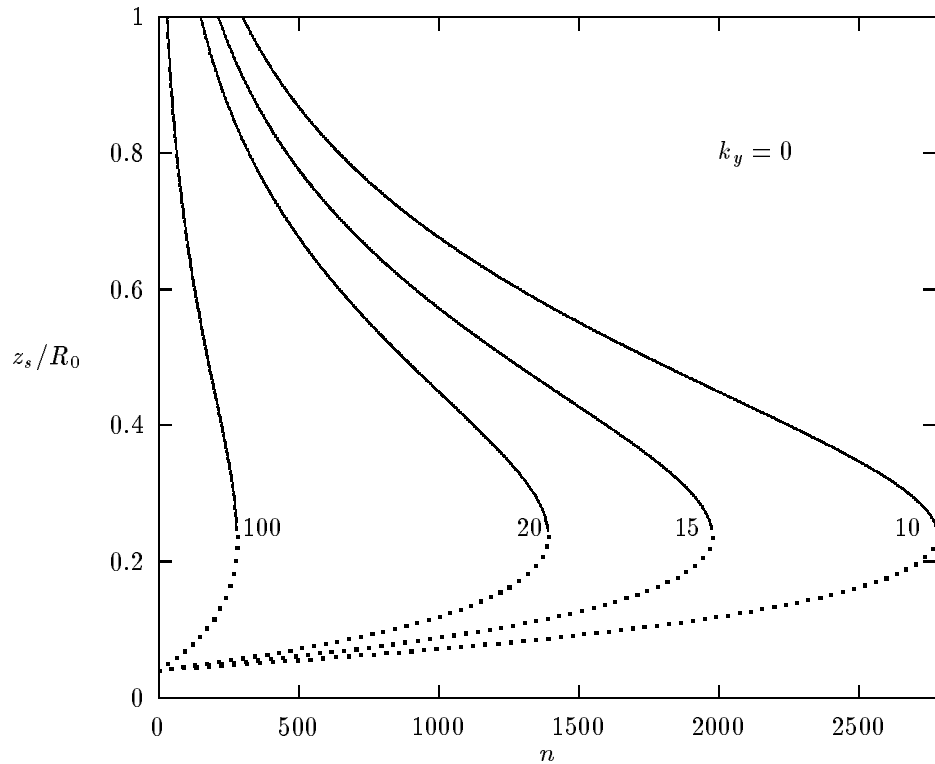


Fig. 5a. The Alfvén resonant layer position $z_s(n)$ for the longitudinal wave propagation $k_y = 0$ in dependence on node numbers n for the ambient magnetic field values $B_0 = 10 \div 100$ G. Dashed curves respond to too low frequency branches $T = f^{-1} \geq T_\odot$ beyond the approximation of the Sun at rest, $T \ll T_\odot = 27$ days.

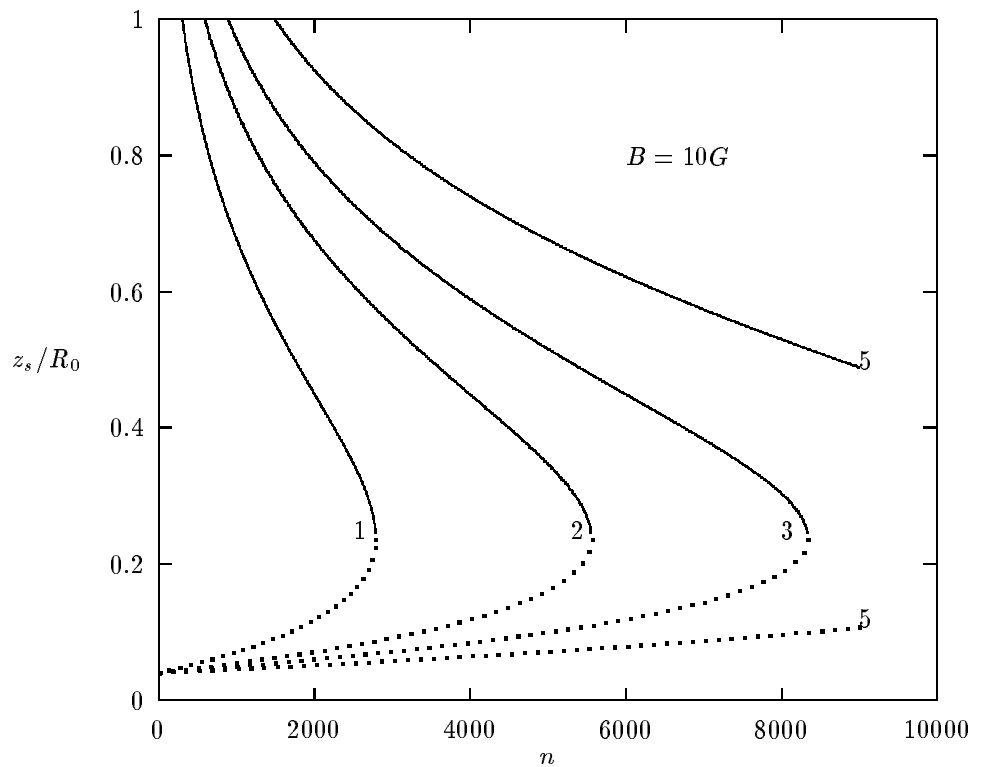


Fig. 5b. The Alfvén resonant layer position $z_s(n)$ for the fixed background field $B_0 = 10 G$ in dependence on the wave propagation angles, $(\cos \alpha)^{-1} = k_\perp/k_x = 1, 2, 3, 5$.

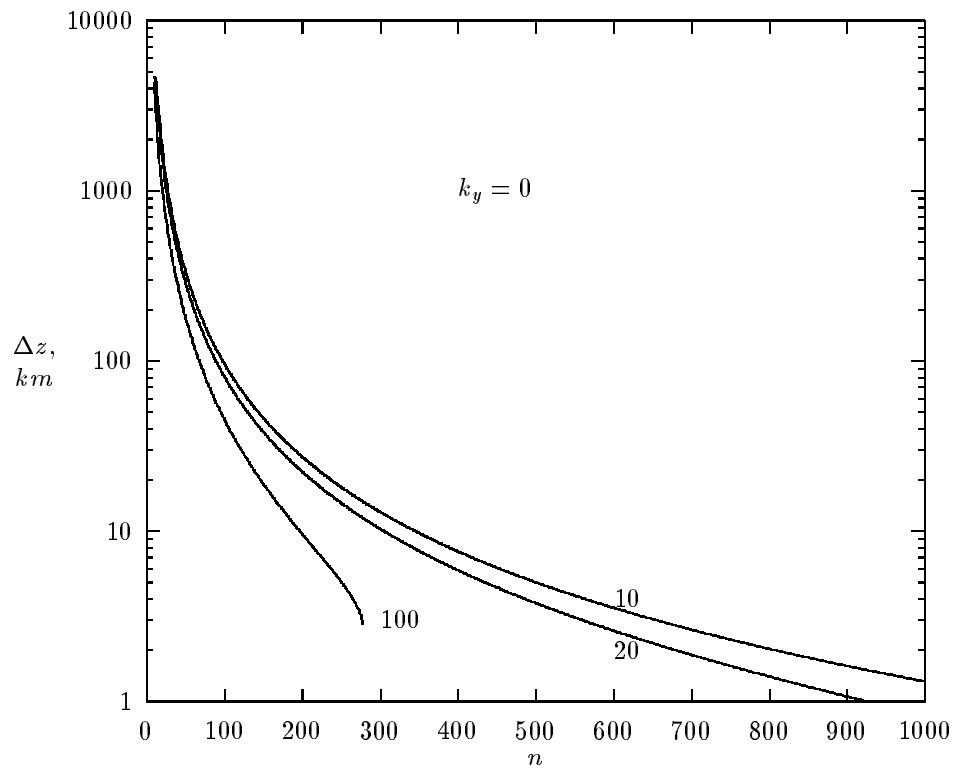


Fig. 6. The width $\Delta z_s(n)$ of Alfvén resonant layers for the longitudinal wave propagation $k_y = 0$ in dependence on the node number n for the ambient magnetic field values $B_0 = 10, 20, 100$ G.

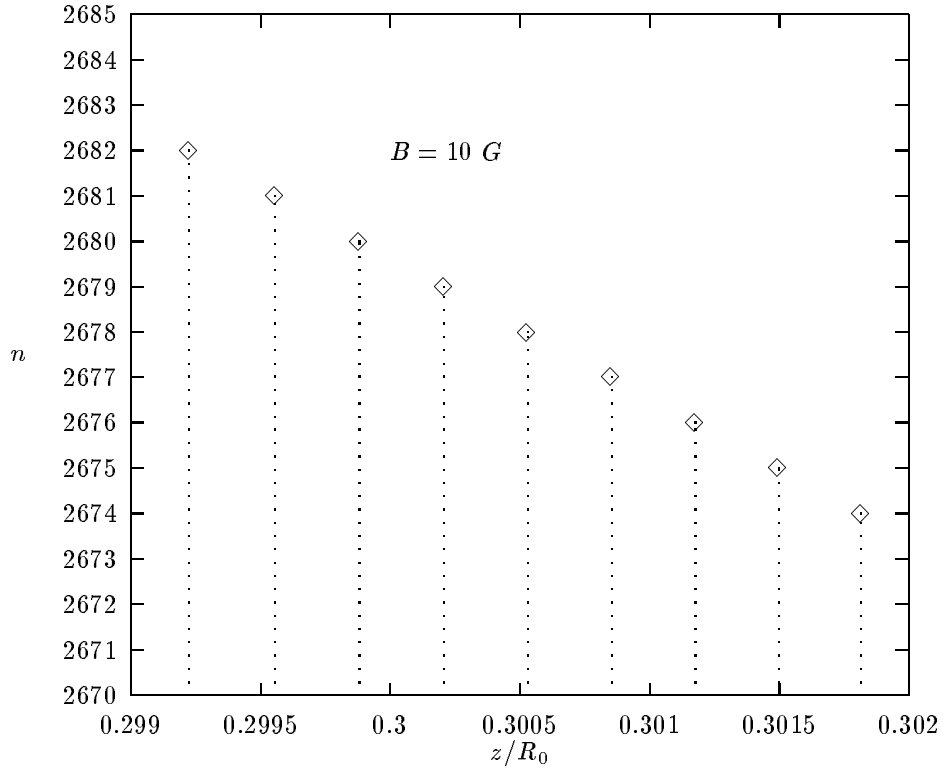


Fig. 7a. The positions $z_s(n)$ for Alfvén resonant layers near the MSW resonant region $z_{MSW} \approx 0.3R_\odot$ for the ambient magnetic field $B_0 = 10 G$. The distance between neighbouring layers equals to $z_s(n-1) - z_s(n) \sim 200 km$.

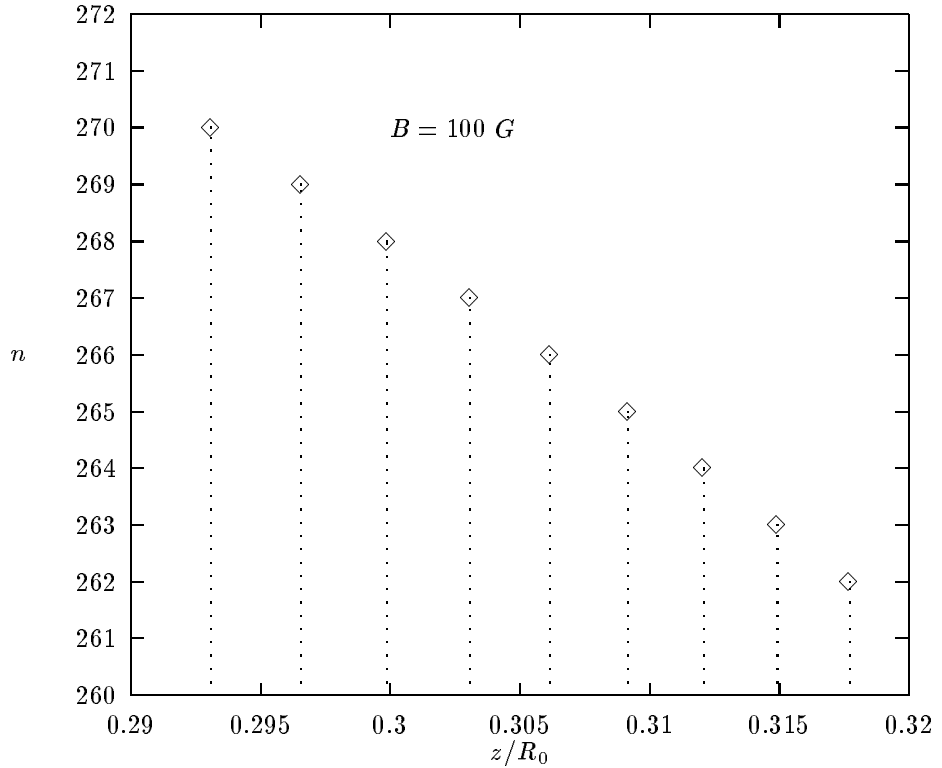


Fig. 7b. The positions $z_s(n)$ for Alfvén resonant layers near the MSW resonant region $z_{MSW} \approx 0.3R_\odot$ for the ambient magnetic field $B_0 = 100 G$. The distance between neighbouring layers equals to $z_s(n-1) - z_s(n) \approx 2000 km$.

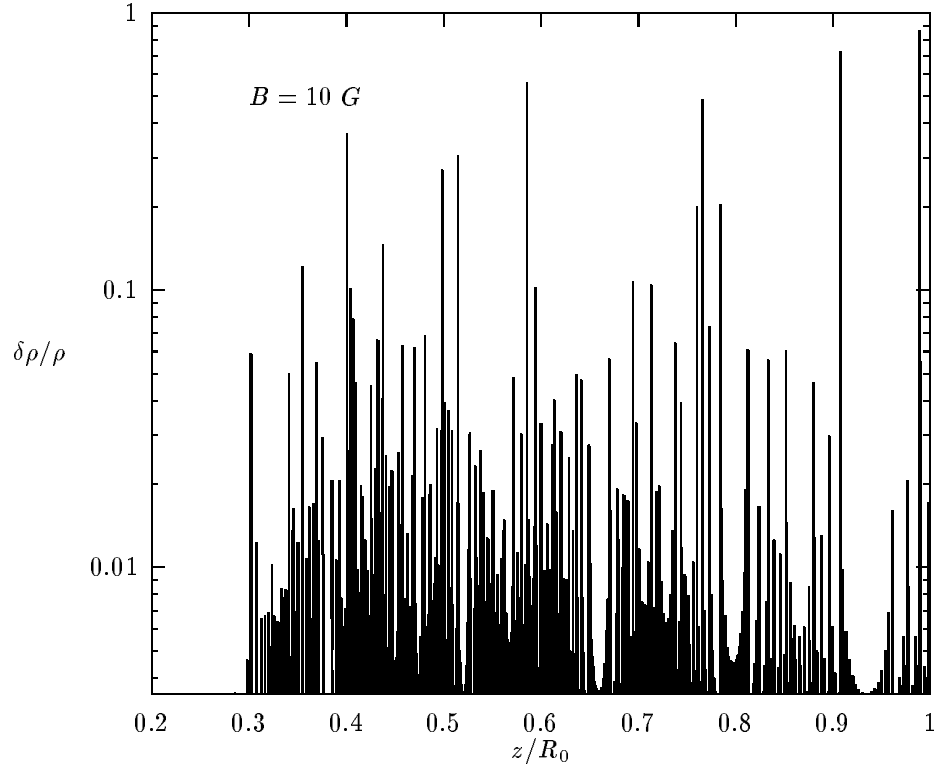


Fig. 8a. The density profile $\delta\rho(z)/\rho_0(z)$ in the case of longitudinal wave propagation $k_y = 0$. The spikes (with unnormalized amplitudes) respond to Alfvén resonant layers with the node numbers for the ambient magnetic field $B_0 = 10$ G from $n \sim 300$ near the surface $z_s = R_\odot$ upto $n = 2680$ at the MSW region $z_s = 0.3R_\odot$. Small amplitudes of regular MAG waves that fill each cavity from the center of the Sun upto the corresponding right boundary $z_s(n)$ (upto a spike) are not seen between spikes while really the wave length within an inner cavity, $\lambda_z = 2\pi/k_z = z_s/n$, is very short since $n \gg 1$.

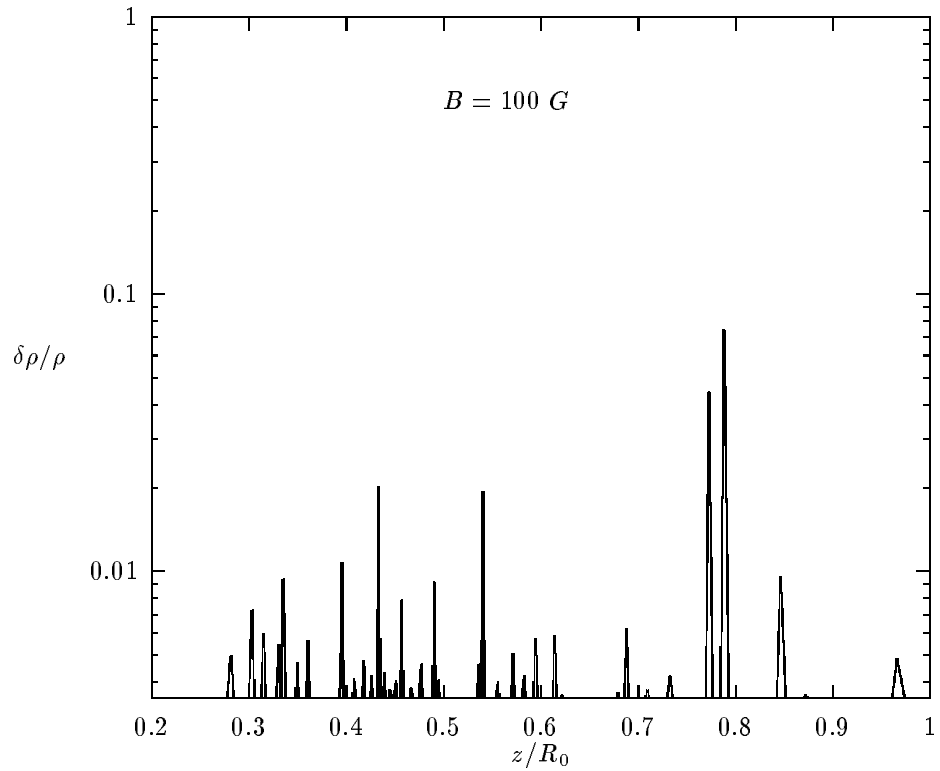


Fig. 8b. The density profile $\delta\rho(z)/\rho_0(z)$ in the case of longitudinal wave propagation $k_y = 0$. The spikes (with unnormalized amplitudes) respond to Alfvén resonant layers with the node numbers for the ambient (large-scale) field $B_0 = 100 \text{ G}$ from $n \sim \text{tens}$ at the surface $z_s = R_\odot$ upto $n = 268$ at the MSW resonant point $z_{MSW} = 0.3R_\odot$.

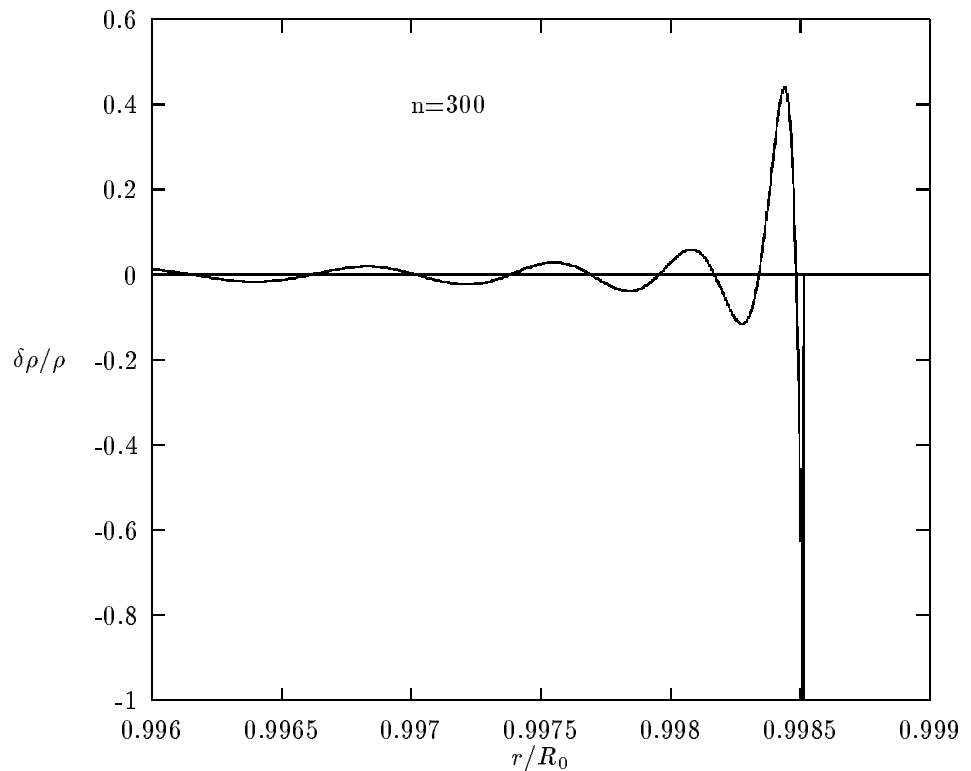


Fig. 9a. The density perturbation profile $\delta\rho_n(z)/\rho_0$ for the wave mode $n = 300$ in the background field $B_0 = 10$ G within the largest cavity with the upper bound near the surface, $z_s/R_\odot \sim 0.99$ (not seen on the large scale $0 \leq z \leq R_\odot$).

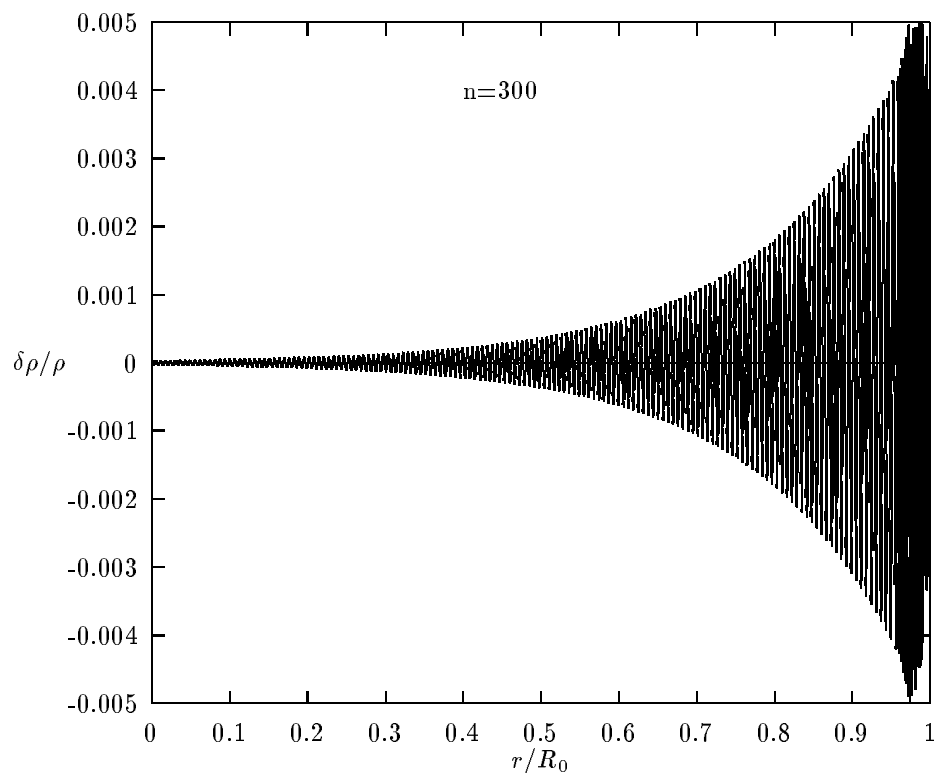


Fig. 9b. Small-scale structure of the same density perturbation mode (Fig.9a) near the resonant layer position $z_s/R_\odot = 0.9985$.